Journal of Hydrology 563 (2018) 1092–1110

Contents lists available at ScienceDirect

Journal of Hydrology

journal homepage: www.elsevier.com/locate/jhydrol

# Spatial interpolation of precipitation from multiple rain gauge networks and weather radar data for operational applications in Alpine catchments

Alain Foehn[a,*], Javier García Hernández[b], Bettina Schaefli[c], Giovanni De Cesare[a]

[a] Laboratoire de Constructions Hydrauliques (LCH), School of Architecture, Civil and Environmental Engineering (ENAC), Ecole Polytechnique Fédérale de Lausanne (EPFL), Switzerland
[b] Centre de recherche sur l'environnement alpin (CREALP), Switzerland
[c] Institute of Earth Surface Dynamics (IDYST), University of Lausanne (UNIL), Switzerland

ARTICLE INFO

This manuscript was handled by Marco Borga, Editor-in-Chief, with the assistance of Francesco Marra, Associate Editor

*Keywords:*
Precipitation
Regression co-kriging
Rain gauge
Weather radar
Spatial interpolation
Alpine catchment

ABSTRACT

Increasing meteorological data availability and quality implies an adaptation of the interpolation methods for data combination. In this paper, we propose a new method to efficiently combine weather radar data with data from two heated rain gauge networks of different quality. The two networks being non-collocated (no common location between the two networks), pseudo cross-variograms are used to compute the linear model of coregionalization for kriging computation. This allows considering the two networks independently in a co-kriging approach. The methodology is applied to the Upper Rhône River basin, an Alpine catchment in Switzerland with a complex topography and an area of about 5300 km$^2$. The analysis explores the newly proposed Regression co-kriging approach, in which two independent rain gauge networks are considered as primary and secondary kriging variables. Regression co-kriging is compared to four other methods, including the commonly applied Inverse distance weighting method used as baseline scenario. Incorporation of additional networks located within and around the target region in the interpolation computation is also explored. The results firstly demonstrate the added value of the radar information as compared to using only ground stations. As compared to Regression kriging using only the network of highest quality, the Regression co-kriging method using both networks slightly increases the performance. A key outcome of the study is that Regression co-kriging performs better than Inverse distance weighting even for the data availability scenario when the radar network was providing lower quality radar data over the studied basin. The results and discussion underline that combining meteorological information from different rain gauge networks with different equipments remains challenging for operational purposes. Future research in this field should in particular focus on additional pre-processing of the radar data to account for example for areas of low visibility of the weather radars due to the topography.

## 1. Introduction

In Switzerland, severe flooding events in recent decades have increased the need for reliable forecasting systems to mitigate flood effects. In 1999, the research project MINERVE (Jordan, 2007a,b; Jordan et al., 2010; Jordan et al., 2012; García Hernández et al., 2007, 2009; García Hernández, 2011a,b; Bérod, 2013) was initiated with the objective of developing a flood forecasting and management system for the Upper Rhône River basin upstream of Lake Geneva (Hingray et al., 2010; Foehn et al., 2016). After the major flood of October 2000 in the Canton of Valais (Switzerland), the need for such a system has increased and since 2013, a forecasting system is operational for the entire basin and used as a tool for decision-making tasks (García Hernández et al., 2014).

Since the beginning of the forecasting system development, enhancing the estimation of the spatial precipitation distribution has been identified as essential (Jordan, 2007a; García Hernández, 2011a; Tobin, 2012). Indeed, to accurately predict flooding induced by heavy precipitation, it is crucial to estimate with good accuracy the causative precipitation (Sikorska and Seibert, 2018). Two main data sources are usually considered: rain gauges (point observations) and weather radars (spatial information). Combining these two data types has been shown to produce improved precipitation estimates (Foehn et al., 2016; Sideris et al., 2014a; Goudenhoofdt and Delobbe, 2009; Jewell and Gaussiat, 2015) for flood forecasting and hydrological modelling in general.

Rain gauges provide direct precipitation measurements which can be fairly accurate; but point observations are heterogeneously distributed over the domain and typically do not cover the entire elevation

* Corresponding author.
*E-mail address:* alain.foehn@epfl.ch (A. Foehn).

https://doi.org/10.1016/j.jhydrol.2018.05.027
Received 13 November 2017; Received in revised form 4 May 2018; Accepted 10 May 2018
Available online 23 May 2018

range of Alpine basins. They are also subject to various sources of error and uncertainty (Villarini and Krajewski, 2010; Cecinati et al., 2017a), such as wind-induced measurement errors (Nešpor and Sevruk, 1999), evaporation and wetting errors (Upton and Rahimi, 2003) or heating-related losses for heated tipping-buckets (Savina et al., 2012). In addition, rain gauge values have to be considered to be spatially representative of their surrounding area, which is a strong hypothesis, in particular for short-time scales (Ciach and Krajewski, 1999; Villarini et al., 2008).

Weather radars, alternatively, provide a better spatial coverage but require a relatively sophisticated post-treatment of the signal backscattered by the precipitation particles and are subject to significant bias and many sources of error (Germann et al., 2006; Germann et al., 2009; Berne and Krajewski, 2013). Radar estimates are in general well correlated both in space and time with rain gauge data, particularly for long accumulation periods but this correlation tends to decrease for sub-hourly accumulation periods (Sideris et al., 2014a).

A wide range of precipitation interpolation methods has been proposed in the literature for rain gauge data interpolation or radar-gauge combination, from rather simplistic methods such as Thiessen polygons (Thiessen, 1911) or Inverse distance weighting (Shepard, 1968) to more sophisticated methods such as simple and multiple linear regressions (Di Piazza et al., 2011), copulas (Vogl et al., 2012) and the wide range of geostatistical methods (Creutin et al., 1988). Univariate geostatistical methods (e.g. simple or ordinary kriging) generally tend to smooth the interpolated variable and therefore struggle to accurately reproduce spatial variability. Multivariate geostatistical methods use additional spatial information from either static (e.g. elevation) or dynamic (e.g. weather radar) covariates to improve the interpolation performance (Wagner et al., 2012). Different approaches of multivariate geostatistics applied to precipitations have been explored in the literature, including Kriging with external drift (KED) (Cantet, 2017), Co-kriging (Goovaerts, 2000), Conditional merging (Ehret, 2003) or Bayesian kriging (Verdin et al., 2015). Ly et al. (2013) propose a methods review for spatial interpolation of daily rainfall data for hydrological modelling at the catchment scale.

Regarding possible covariates (additional information), only few studies really focused on multivariate interpolation of hourly precipitation over Alpine catchments. Schiemann et al. (2011) showed that applying KED to hourly rain gauges and radar data over entire Switzerland performs better than interpolated rain gauge data or radar data alone. For flatter areas, Haberlandt (2007) has shown over the Elbe basin, in Germany, that for hourly precipitation, the most important additional information was the radar, followed by daily precipitation observations of a denser network with lower temporal resolution, and finally the elevation, which was considered "to play only a secondary role" in the studied case. Goovaerts (2000) reported that incorporating elevation can improve spatial interpolation of monthly and yearly rainfall when applied to a basin in Southern Portugal. Ly et al. (2011) analyzed the integration of elevation in KED and Ordinary Co-kriging and concluded that it did not improve the interpolation accuracy for daily rainfall over a basin in Belgium. These observations tend to agree with Bárdossy and Pegram (2013), who found over three regions in Germany that "correlation between precipitation and topography increases with the length of time interval". Sikorska and Seibert (2018) showed that radar-based daily precipitation estimates, adjusted to precipitation rates from ground stations, provided better flood predictions as compared to using only rain gauges observations.

Sideris et al. (2014a) proposed a methodology applied in Switzerland in which rain gauges were combined with weather radar data using data from the time step of interpolation as well as from the preceding time step (as secondary co-kriged variable) in a co-kriging with external drift (CED) approach. Comparing their spatio-temporal method with a classical KED approach, they concluded that the skill scores were similar when considering an aggregation time of 60 min. However, for shorter aggregation periods (10–30 min), CED resulted in higher performance values than KED. This methodology is used for the computation of the *CombiPrecip* product (MeteoSwiss, 2014a), the operational hourly spatialized precipitation product of the Swiss Federal Office of Meteorology and Climatology (MeteoSwiss).

Numerical weather forecasts can also represent an alternative covariate. Tobin et al. (2011) have applied KED for interpolation of precipitation and temperature in Switzerland using (i) elevation and (ii) the COSMO7 weather forecast product of MeteoSwiss (MeteoSwiss, 2017). Whereas temperature measurements were found to be "strongly correlated with the closest COSMO7 grid point" at an hourly time step, good correlation between measurements and COSMO7 estimates was observed for precipitation only for "cumulative data over the event". Tobin et al. (2011) thus proposed to use an event averaged linear drift for precipitation interpolation. Compared to Inverse distance weighting (IDW) and Ordinary kriging (OK), KED with elevation tended to produce the least biased estimation in their study. In terms of error, OK and both KED methods using elevation and the COSMO7 data had similar scores and outperformed IDW. However, when looking only at stations above 1500 m asl., KED with COSMO7 showed the highest error for their case study in Switzerland.

Covariates can also be processed before being used in combination with rain gauge data. Berndt et al. (2014) showed that smoothing radar data both spatially with the adjacent cells or/and temporally over several time steps improved the performance of merging rain gauges and radar data. Instead of always using the radar pixel containing a rain gauge, Sideris et al. (2014b) incorporated in the *CombiPrecip* product a convection control routine, in which the coefficient of dispersion over the 25 pixels around the rain gauge pixel is computed. When a certain threshold is exceeded, the value of the pixel with the closest value to the rain gauge within the 25 pixels is used for the merging.

Commercial microwave link networks have also been explored over the last decade as a supplementary source of precipitation data (Messer et al., 2006). Hydrological applications show a great potential of this approach, in particular in poorly equipped areas (Smiatek et al., 2017).

Besides providing a reliable radar-rain gauge combination for the target region, the objective of this paper is to assess in detail what gain can be expected from combining the most recent radar data for precipitation interpolation with rain gauge data from two ground-based networks of different data quality. This includes a comparison to the commonly used deterministic Inverse distance weighting method applied to rain gauge data as baseline scenario. Another key question is the quality of the radar-gauge combination methodology if applied to the data situation prevailing before the installation of a new weather radar covering the studied basin in 2014. Using the data from the already existing other Swiss weather radars, such an application allows computing series over a longer time period which is required for hydrological modelling purposes. Finally, the paper also aims at analyzing the effect of incorporating additional station networks located within and around the target region in the interpolation computation.

## 2. Study region and data

### 2.1. Hydrological basin

The studied area corresponds to the Upper Rhône river basin, defined as the hydrological basin between the Rhône Glacier (on the east) and Lake Geneva (on the west). The area is 5351 km$^2$ (Fig. 1) and the elevation varies from 372 m asl. at the outlet to 4'634 m asl. on the top of the Dufourspitze, with a mean elevation of 2158 m asl. (Fig. S.1 in Supplementary material). The area above 3000 m asl. represents 13.0% of the area, whereas the part above 4000 m asl. only covers 0.3% of the total area. The glacierized area has been estimated to 569.2 km$^2$ in 2010 (Fischer et al., 2015), which corresponds to about 10.6% of the total area.

Yearly precipitation intensities are spatially variable over the basin. The yearly average over the period 1981–2010 is of 603 mm for the

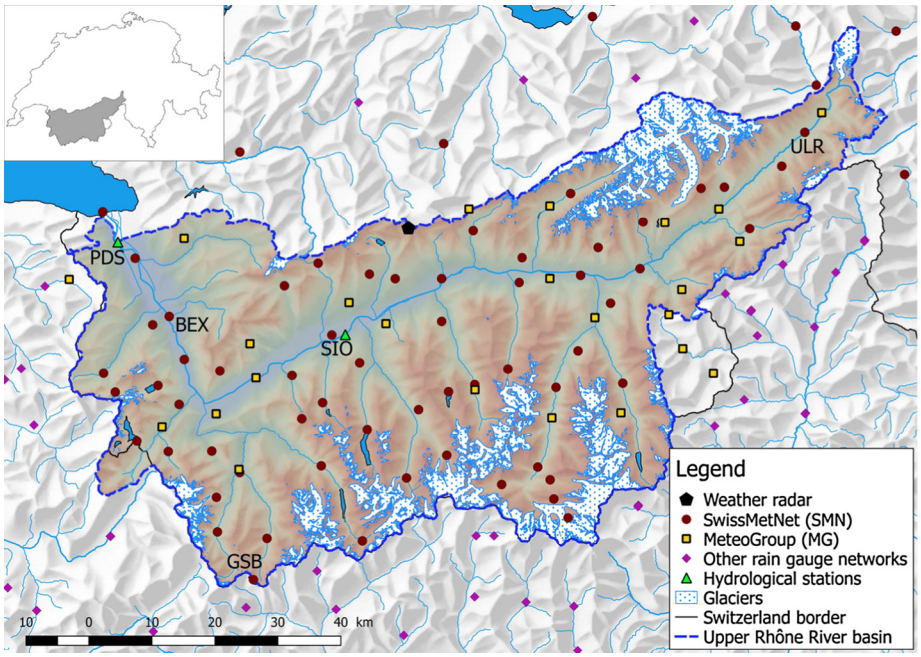


**Fig. 1.** Location of the MeteoSwiss, MeteoGroup and surrounding meteorological networks, as well as the Pointe de la Plaine Morte weather radar and a selection of hydrological stations. Abbreviations indicate the MeteoSwiss stations Sion (SIO), Col du Grand St-Bernard (GSB), Bex (BEX) and Ulrichen (ULR) as well as the hydrological stations Sion (SIO) and Porte du Scex (PDS). Glaciers and principal rivers are also shown. (Topographic data source: Swisstopo (2017a) for rivers and lakes, Swisstopo (2013) for the glaciers (with modifications), Swisstopo (2005) for the DEM, Swisstopo (2012) for the relief and Swisstopo (2017b) for the national boundary line).

station Sion (SIO), at 482 m asl. and located near the center of the basin (Fig. 1), whereas the station at Col du Grand St-Bernard (GSB), on the south-western border and situated at 2472 m asl., reported an average of 2368 mm per year over the same period (MeteoSwiss, 2014b). Precipitation is observed all year long, with a monthly average minimum and maximum of 35 mm (April) to 64 mm (December) for SIO and 135 mm (July) to 248 mm (November) for GSB. Depending on the elevation, the solid precipitation fraction can represent a significant proportion of the annual precipitation.

### 2.2. Rain gauges data within the basin

Several networks of rain gauges are available within the basin, but only the two networks with heated rain gauges have been considered for this study, in order to make the methodology applicable all year round. The first one is the SwissMetNet (MeteoSwiss, 2016a) network of MeteoSwiss, hereafter refereed as SMN. The SMN data are based on reliable equipment and subject to a serious quality control (Musa et al., 2003). On July 1st, 2013, 40 SMN stations were operational within the basin. This number had increased to 58 on March 1st, 2017, which represents an average area per station of 92 $km^2$, which makes it a particularly dense network. As a comparison, on the same date, the Swiss average was 168 $km^2$ per station and values reported by other authors tend to be higher: about 571 $km^2$ per station in Germany (Berndt et al., 2014) or 135 $km^2$ in the Wallon region, where Goudenhoofdt and Delobbe (2009) described the network as “dense”. A complete list of used SMN stations is given in Tables S.1 and S.2 (Supp. Mat.).

For the analysis, all available stations have been considered in each event, regardless whether the station was available or not for the other events. This implies that the number of stations considered for the computation increases over the events between 2012 and 2017. Table 1 lists the equipment used in the different networks (MeteoSwiss, 2015) and the number of stations.

The second network is composed of 23 stations of the private company MeteoGroup Switzerland AG, hereafter refereed as MG. More stations of this network are available within the basin, but data from only 23 stations were available for the present study, which have been selected to supplement SMN stations over uncovered areas. A complete list of used MG stations is given in Table S.3 (Supp. Mat.).

Combined with the SMN stations, the average area per station over the basin drops to 66 $km^2$. The elevation range is 381–2472 m asl. for the SMN stations and 460–2347 m. asl for the MG stations, with median elevations of respectively 1537 and 1365 m. asl.

The analysis of the data has shown a tendency of MG stations to report less precipitation than the SMN stations, with differences largely exceeding 20% for some hourly time steps. Similar observations had been made by MeteoSwiss when comparing their manual daily precipitation measurements with automatic observations from MeteoGroup stations (J. Fisler, MeteoSwiss, personal communication, January 9, 2017). In the field intercomparison of rain intensity gauges realized by Vuerich et al. (2009) for the account of the World Meteorological Organization (WMO), all three concerned station types, or their predecessor (for the OTT equipment), had been tested (Lanza and Vuerich, 2009). The stations used by MeteoSwiss were evaluated as “satisfactory” (Lambrecht) and “very good” (OTT), whereas the stations installed by MeteoGroup (Davis) were evaluated as “insufficient”. Based on these conclusions, the SMN stations have been defined for this study as being the “primary” network and the MG stations as the “secondary” network. This distinction will be considered when using data from both networks. It is worth mentioning here that neither the MeteoSwiss nor the MeteoGroup station data are corrected for undercatch of solid precipitation, which is known to have an effect on solid precipitation intensity estimation in mountainous regions (Egli et al., 2009).

### 2.3. Rain gauges data around the basin

In addition to the presented two networks located within the basin (81 stations) and their 12 stations located around the basin (Table 1), 62 stations of networks located around the basin and equipped with heated rain gauges have been considered (Table 1). This additional information allows a better estimation at the border of the basin as well as a more correct estimation of the precipitation fields for example in the southern neigbhouring area. This is important as more than half of the meteorological situations having produced more than 110 mm/d of precipitation over 3 days in the Upper Valais since 1975 have originated from souths according to Attinger and Fallot (2003), as cited in Tobin et al. (2011).

**Table 1**
List of considered rain gauge networks and respective characteristics. Number of stations for MeteoSwiss refers to March 1st, 2017.

| Network | Number of stations | Location | Sensor model | Period |
|---|---|---|---|---|
| SwissMetNet (SMN) | 17 (+9) | Basin (+ neighbouring cantons) | *1518 H3* and *15188* by Lambrecht (tipping bucket) | 2012–2017 |
| SwissMetNet (SMN) | 41 (+2) | Basin (+ neighbouring cantons) | *Pluvio*$^2$ by Ott (weighing principle) | 2012–2017 |
| MeteoGroup (MG) | 23 (+1) | Basin (+ France) | *Rain Collector II* by Davis (tipping bucket) | 2012–2017 |
| Kanton Bern | 11 | Bern (Switzerland) | Unknown (heated) | 2012–2017 |
| MeteoFrance | 5 | France | Unknown (heated) | 2012–2017 |
| EDF | 10 | France | Unknown (heated) | 2012–2016 |
| Regione Autonoma Valle d'Aosta | 25 | Italy | Unknown (heated) | 2012–2017 |
| ARPA Piemonte | 11 | Italy | Unknown (heated) | 2012–2015 |

### 2.4. Weather radar data

MeteoSwiss has operated since 1995 three weather radars covering the entire national territory of Switzerland (MeteoSwiss, 2016b), modernized in 2011 and 2012 with new technologies (MeteoSwiss, 2012). In May 2014, a fourth installation has been inaugurated at the Pointe de la Plaine Morte (see Fig. 1), within the basin studied in here (MeteoSwiss, 2014c), followed two years later by a fifth radar in the Eastern part of Switzerland (MeteoSwiss, 2016c) (Fig. S.2, Supp. Mat.). The radar of Pointe de la Plaine Morte is officially operational since June 2014. The two additional radars contributed to a better radar coverage of Alpine regions (Germann et al., 2015). The back-scattered signal measured by the five dual-polarization Doppler C-band radars (Gabella, 2017) is transformed into rain rate estimates through several procedures, described in Germann et al. (2006). Radar precipitation estimates are generated every 5 min over a 1-km resolution raster based on a combination of the data of the available radars over Switzeraland. For the present study, the hourly aggregated radar precipitation estimates product of MeteoSwiss is used, classified into 256 categories. The production routine of the product had been optimized by MeteoSwiss for the configuration with 3 weather radars in Switzerland. A new radar precipitation estimates product is generated by MeteoSwiss since February 2018, but no historical data are yet available (MeteoSwiss, personal communication, March 7, 2018).

It is worth pointing out that the highly mountainous aspect of the studied basin implies an accuracy loss of the radar estimate as compared to flatlands (Erdin et al., 2012). Beam shielding by mountain ranges is certainly one of the major issues, as discussed later in Section 5. To reduce this effect, a fixed adjustment map computed based on a long-term comparison between weather radar estimation and rain gauge measurements is used by MeteoSwiss in the computation of their radar precipitation estimates product (Germann et al., 2006). However, this long-term comparison-based correction does not consider the data of the two newly installed radars. Positive effect on the basin of interest is therefore probably lower than for some other regions of Switzerland. Ground echoes elimination also requires a proper pre-treatment of the data. In addition, radar data suffer of bias issue, by over- or undershooting the precipitation. This is why they are combined with rain gauges to properly adjust the precipitation field. Furthermore, solid precipitation estimation is known to be more challenging than the liquid phase, resulting in better detection performance in summer than in winter (Speirs et al., 2017), whereas melting snow tends to enhance the back-scattered signal (Germann et al., 2006).

### 2.5. Events description

The main analysis is carried out on four events that occurred over the period of data availability for the meteorological radar of Pointe de la Plaine Morte (2014–2017). Additionally, two events in 2012 and 2013, corresponding to the highest peak flow in the basin over the 2008–2017 period, as well as an event in July 2014 during which the radar of Pointe de la Plaine Morte was temporary not operating, are also considered to discuss the performance of the methodology before the installation of the radar of Pointe de la Plaine Morte. This is important as data over several years are necessary when using the interpolated data for hydrological model calibration.

The four events considered for the main analysis cover different seasons and were chosen for their high precipitation accumulation over the events. The period for each event has been defined such as to start two hours before the first hour with at least four SMN stations reporting at least 1.5 mm/h, and to stop two hours after the last hour respecting this condition; interruptions of less than 12 h of the above mentioned condition were considered to be part of the same event.

The characteristics of the events are given in Table 2 and presented hereafter, listed in chronological order. The median and maximum accumulation values are computed from the rain gauge values. The snow line elevation has been estimated from archives of short term weather forecasts of MeteoSwiss. In fact, even if recent developments

**Table 2**
Characteristics of the seven analyzed events.

| Event identifier | A | B | C | 1 | 2 | 3 | 4 |
|---|---|---|---|---|---|---|---|
| Year | 2012 | 2013 | 2014 | 2014 | 2015 | 2016 | 2017 |
| Start [day.month Time] | 1.7 12:00 | 28.7 21:00 | 28.7 11:00 | 4.11 08:00 | 30.4 22:00 | 10.1 07:00 | 5.3 15:00 |
| End [day.month Time] | 2.7 16:00 | 29.7 17:00 | 29.7 15:00 | 6.11 04:00 | 4.5 10:00 | 13.1 04:00 | 7.3 13:00 |
| Duration [h] | 28 | 20 | 28 | 44 | 84 | 69 | 46 |
| Season | Summer | Summer | Summer | Fall | Spring | Winter | Winter |
| Approx. snow line elevation [m asl.] | 3200–3400 | 2600 | 2500–3100 | 800–2000 | 1800–2600 | 800–1400 | 700–1400 |
| Plaine Morte radar data | No | No | No | Yes | Yes | Yes | Yes |
| Median accumulation at stations [mm] | 24.3 | 39.3 | 45.5 | 37.5 | 96.2 | 41.2 | 34 |
| Maximum accumulation at a station [mm] | 65.3 | 69.7 | 62.7 | 179.5 | 375.7 | 158 | 150.7 |
| SMN stations (number) | 28 | 40 | 52 | 52 | 52 | 55 | 58 |
| MG stations (number) | 20 | 22 | 23 | 23 | 23 | 23 | 23 |
| Qmax at Sion [$m^3/s$] | 703 | 708 | 394 | 146 | 231 | 64 | 53 |
| Qmax at Porte du Scex [$m^3/s$] | 864 | 901 | 537 | 272 | 606 | 191 | 139 |

enable hydrometeor type analysis from radar data (Grazioli et al., 2015), snow line elevations cannot yet be estimated directly from the radar data. Return periods are provided by MeteoSwiss (2016d) from which only statistically robust results were considered. Peak discharges (Qmax) and corresponding return periods of the events at the hydrometric stations of the Federal Office for the Environment (FOEN, 2017a,b) in Sion and in Porte du Scex, at the outlet of the basin (Fig. 1), are also indicated in Table 2 and discussed hereafter where relevant. All times are given in UTC + 1.

#### 2.5.1. Events without Pointe de la Plaine Morte data

*Event A*: 1.7.2012 12:00 to 2.7.2012 16:00.

The event of July 2012 mostly concerned the eastern part of the basin. The overall precipitation was not particularly intense, with a median accumulation over all the stations of 24.3 mm, but with a snow line elevation reaching 3400 m asl., most of the precipitation fell as rain. This resulted in a peak discharge in the Rhône at Sion of 703 $m^3/s$ on 2 July (FOEN, 2017b), corresponding to an estimated return period of 20 years according to FOEN (2017a).

*Event B*: 28.7.2013 21:00 to 29.7.2013 17:00.

The event of July 2013 touched the entire basin with locally intense storms (median accumulation of 39.3 mm). The high snow line elevation, situated at about 2600 m asl., resulted in a high proportion of rainfall, which led to a peak discharges of 708 $m^3/s$ in Sion and 901 $m^3/s$ in Porte du Scex on 29 July (FOEN, 2017b). The return period of the discharge in Sion was estimated to 21 years (FOEN, 2017a).

*Event C*: 28.7.2014 11:00 to 29.7.2014 15:00.

A westerly depression affected the entire basin and particularly its western part. The median accumulation reached 45.5 mm over the event. The snow line elevation varied between around 2500 and 3100 m asl. Compared to the events in 2012 and 2013, the intense precipitation was less concentrated in time, probably partially explaining why the resulting flow in downstream rivers did not reach values as high as in 2012 and 2013 (see Table 2). The event has the particularity of having taken place after the entry into service of the radar of Pointe de la Plaine Morte, but with the mentioned radar not being in operation over the event (temporary interruption). This offers a station density close to the maximum density of 2017 with a radar data configuration corresponding to the one of before 2014 (without the radar of Pointe de la Plaine Morte), which is interesting for analysis purposes.

#### 2.5.2. Events including Pointe de la Plaine Morte data

*Event 1*: 4.11.2014 08:00 to 6.11.2014 04:00.

An active westerly disturbance with polar air resulted in heavy precipitation mostly in the Eastern part of the basin. The median accumulation over the 44 h was 37.5 mm but station Ulrichen (Fig. 1) reported for example 96.2 mm over 16 h, corresponding to a return period of 18 years according to MeteoSwiss (2016d). The snow limit varied between 800 and 2000 m asl.

*Event 2*: 30.04.2015 22:00 to 4.5.2015 10:00.

A heavy precipitation event coming from the west with air relatively mild and very humid reached Switzerland, with successive precipitation fronts. The snow limit varied between 1800 and 2600 m asl. The median accumulation was 96.2 mm for a maximum accumulation over the 84 h of 375.7 mm (in station Clusanfe). In terms of return period, the station Bex (Fig. 1), in the western part of the basin, reported a rainfall accumulation of 100.9 mm over 3 days, corresponding to a return period of 58 years. Other stations within the basin reported accumulation with return periods exceeding 10 years.

*Event 3*: 10.1.2016 07:00 to 13.1.2016 04:00.

A series of disturbances reached Switzerland from the west with heavy snowfalls on the Alps, exceeding in some places 100 cm of fresh snow over the 3 days. The snow limit varied between 800 and 1400 m asl and the median liquid-equivalent precipitation was 41.2 mm.

*Event 4*: 5.3.2017 15:00 to 7.3.2017 13:00.

Strong westerly winds resulted in successive fronts towards the Swiss Alps, with a median precipitation of 34 mm. The snow limit varied between 700 and 1400 m asl. over the event, thus a large fraction of the precipitation fell as snow.

## 3. Methodology

The high spatial variability of precipitation implies the use of methods capable of analyzing and reproducing as reliably as possible the spatial pattern of the precipitation fields. On one side, the interpolation method should be efficient in combining the available rain gauge and radar data, considering different networks of ground stations. On the other side, for being used operationally, it should not imply long computational time and must work on an automatic basis.

### 3.1. Estimation methods

Five different estimation methods are compared within this work, ranging from commonly used methods to the newly proposed one handling with two non-collocated rain gauge networks of varying quality. The first method is the so-called Inverse distance weighting method (Shepard, 1968), hereafter referred to as IDW, currently used within the MINERVE forecasting system and therefore considered as the baseline scenario. This method only uses the rain gauge data. The second method considers directly the raw radar value over the entire basin. The three other methods combine rain gauge and radar data by applying a multiplying coefficient to the radar raster, based on a linear regression of the radar data on the rain gauge data, to obtain a trend ("corrected radar"). Residuals, defined as the difference between the value observed at a rain gauge and the value of the containing pixel of the trend, are then computed at each gauge location before being interpolated. The way this interpolation is carried out differentiates the three last methods. The first one is applying IDW to the residuals, whereas the two others are based on a kriging approach (Webster and Oliver, 2007; Delhomme, 1978). Finally, interpolated residuals are added to the trend to get the final product. Table 3 summarizes the five methods.

The implementation has been done on the R language and environment for statistical computing (R Core Team, 2016). For the three regression methods, the methodology and nomenclature is partly based on Sideris et al. (2014a).

#### 3.1.1. Inverse distance weighting (IDW)

The Inverse distance weighting method (Shepard, 1968) is a deterministic interpolation method (Ly et al., 2013), in the sense that it does not exploits the statistical properties of the observation sample, thus not providing a prediction error assessment. In general, the aim of interpolation is to estimate the precipitation depth $p$ at an unsampled spatial location $s_0$ with coordinates $(x_0, y_0)$ using the available observation data at rain gauges (see Table 7 for variables list). IDW applies a linear combination of the observations within a research radius

**Table 3**
Estimation methods.

| Name | Short name | Rain gauges | Radar | Remark |
|---|---|---|---|---|
| Inverse distance weighting | IDW | Yes | No | Reference |
| Radar value | Radar | No | Yes | Raw radar data |
| Regression inverse distance weighting | RIDW | Yes | Yes | IDW on residuals |
| Regression kriging | RK | Yes | Yes | Simple kriging on residuals |
| Regression co-kriging | RCK | Yes | Yes | Co-kriging on residuals |

**Table 4**
Summary of the performance indicators.

| Indicator | Min. value | Max. value | Optimal value |
|---|---|---|---|
| Bias | $-\infty$ | $\infty$ | 0 |
| MAD | 0 | $\infty$ | 0 |
| RMSE | 0 | $\infty$ | 0 |
| MRTE | 0 | $\infty$ | 0 |
| Scatter | 0 | $\infty$ | 0 |

$\rho$, with a decreasing influence with increasing distance. The rain gauge measurements vector over a period $t$ is given by:

$$\boldsymbol{g}(t) = [g(s_1, t), g(s_2, t), \ldots, g(s_N, t)] \tag{1}$$

where $N$ is the number of available rain gauge measurements over the period $t$ and $s = (x, y)$ the spatial-coordinate vector of a given point.

The estimated precipitation $\hat{p}(s_0, t)$, at a given location $s_0$, is then given by:

$$\hat{p}(s_0, t) = \begin{cases} g(s_i, t) & \text{if } \exists\ i: d(s_0, s_i) = 0 \\ \frac{\sum_{i=1}^{N} \lambda_i g(s_i, t)}{\sum_{i=1}^{N} \lambda_i} & \text{else } \forall\ i: 0 > d(s_0, s_i) \leqslant \rho \end{cases} \quad \forall\ s_0 \in D \subseteq \mathbb{R}^2 \tag{2}$$

where

$$\lambda_i = \frac{1}{d(s_0, s_i)^{\beta}} \tag{3}$$

with $d$ being the distance between the location of interpolation and the location of observation $i$, $\beta$ a power coefficient, $\rho$ the research radius and $D$ the spatial domain; $\mathbb{R}$ is the set of real numbers. The normalization allows the sum of the weights to equal 1.

### 3.1.2. Radar value (Radar)

The Radar value method consists in using directly the raw radar data as the precipitation estimation over the basin. The quality of the raw radar product can thereby be investigated.

### 3.1.3. Regression inverse distance weighting (RIDW)

In the three remaining methods, from the geostatistical interpolation methods, the radar information is used to compute a trend of the precipitation field with a multiplicative coefficient. It is worth noting here that merging rain gauge and radar data implies several hypotheses (Sideris et al., 2014a). Firstly, it is assumed that for both the rain gauges and the radar estimates, the measured physical quantity is the precipitation depth over spatial blocks of a size equal to the spatial resolution of the radar (1 km$^2$). This ignores the difference in spatial resolution. In complex topographies like in the context of this study, this can have implications due to the limited spatial representativeness of rain gauges. Secondly, the precipitation estimates of the radar over a spatial block of 1 km$^2$ is assumed to reflect the precipitation depth falling on the surface of the same block. This presumes perfect vertical precipitation fluxes and no exchange with adjacent blocks, which is not the case in reality. In addition, it must be noted that the precipitation depth estimates given by the radar can be affected by areas of invisibility due to shielding of the radar beam by mountain ranges. This obviously also impacts the performance of the interpolation.

In addition to the rain gauge measurements vector $\boldsymbol{g}(t)$ defined in the IDW method, the radar precipitation estimates at rain gauge locations over the period $t$ are considered:

$$\boldsymbol{r}(t) = [r(s_1, t), r(s_2, t), \ldots, r(s_N, t)] \tag{4}$$

During the interpolation, radar precipitation estimates at each interpolation point are also used.

In geostatistics, a random process $Z(s, t)$ can be modeled as the sum of a deterministic part $m_Z(s, t)$, corresponding to the average or trend component, and a stochastic residual component $\epsilon(s, t)$, which corresponds to local fluctuations of the trend, so that:

$$Z(s, t) = m_z(s, t) + \epsilon(s, t) \quad \forall\ s \in D \subseteq \mathbb{R}^2; t \in T \subseteq \mathbb{R} \tag{5}$$

where $s$ is the vector of spatial coordinates of a given point and $T$ the temporal domain.

In the context of the present work, Eq. (5) can be rewritten for the precipitation depth $p$ over the entire domain as:

$$p(s, t) = m_p(s, t) + \epsilon(s, t) \tag{6}$$

The trend $m_p(\boldsymbol{s}, t)$ for a spatial coordinates vector $\boldsymbol{s}$ is commonly modeled as a linear function of a smoothly varying external variable (Goovaerts, 1997). In our case, this external variable is the radar $r(\boldsymbol{s}, t)$:

$$m_p(\boldsymbol{s}, t) = a(t) r(\boldsymbol{s}, t) \tag{7}$$

where $a(t)$ is a regression coefficient and $r(\boldsymbol{s}, t)$ is the radar values vector at time $t$. The coefficient $a(t)$ is computed as the slope of a linear regression of all pairs of points composed of the gauge values on the y-axis and the values of the containing radar pixel on the x-axis. $a(t)$ is assumed to be constant spatially in the interest of robustness.

In other methods, such as Kriging with external drift (KED), the trend is computed using two regression parameters (thereby adding also an intercept) and often evaluated within the kriging estimation process itself (e.g. in KED). The choice of a unique parameter has been motivated by the wish of maintaining zero precipitation in the trend where there was no precipitation reported by the radar estimates.

To compute the residuals $\epsilon(\boldsymbol{s}, t)$, the trend $m_p(\boldsymbol{s}, t)$ is subtracted from the observed value at the station locations:

$$\epsilon(\boldsymbol{s}, t) = g(\boldsymbol{s}, t) - m_p(\boldsymbol{s}, t) = g(\boldsymbol{s}, t) - a(t) r(\boldsymbol{s}, t) \tag{8}$$

The residuals $\epsilon(\boldsymbol{s}, t)$ are then interpolated using the inverse distance weighting method to obtain the interpolated residuals $\hat{\epsilon}_{\mathrm{RIDW}}(s_0, t)$ at location $s_0$. The final estimate is obtained by adding the trend $m_p(s_0, t)$ to the interpolated residual:

$$\hat{p}_{\mathrm{RIDW}}(s_0, t) = m_p(s_0, t) + \hat{\epsilon}_{\mathrm{RIDW}}(s_0, t) \quad \forall\ s_0 \in D \subseteq \mathbb{R}^2 \tag{9}$$

Fig. 2 illustrates the different steps of the RIDW method.

### 3.1.4. Regression kriging (RK)

Kriging is a family of interpolation methods in which the covariance between observations is used to define a linear combination of the observations for interpolation. Practically, kriging methods consider the increasing dissimilarity between observations to characterize the spatial structure of the data. One of the conditions to apply the elementary methods of kriging, Simple and Ordinary kriging, is to assume the random variable to be first-order stationary: the expected value is constant over the domain of interpolation. This condition is hardly satisfied when working directly with rain gauge data, as it might rain for example only in one part of the basin. This non-stationarity of the precipitation fields is here addressed by removing a trend based on the radar data so that Simple or Ordinary kriging can be applied to the computed residuals. This is however an approximation as the non-stationarity of the precipitation statistical properties cannot be fully captured by the radar data.

This approach is named Regression kriging (RK) in the present paper, according to the nomenclature in Odeh et al. (1995). Other names have been proposed for similar approaches in the literature: *kriging combined with linear regression* (Ahmed and De Marsily, 1987), *kriging detrended data* (Phillips et al., 1992), *kriging with a trend model* (Goovaerts, 1997) or *residual kriging* (Alsamamra et al., 2009). Hengl et al. (2007) discussed the characteristics of *regression-kriging* and applied the approach to three case studies. RK is somewhat similar to Kriging with external drift (KED), the difference being that the linear regression and the kriging interpolation is done in successive steps in RK and all-at-once in KED. This choice of successive steps allows us to define a subset of stations for (a) the linear regression step, (b) the variogram computation for the spatial interpolation of the residuals and

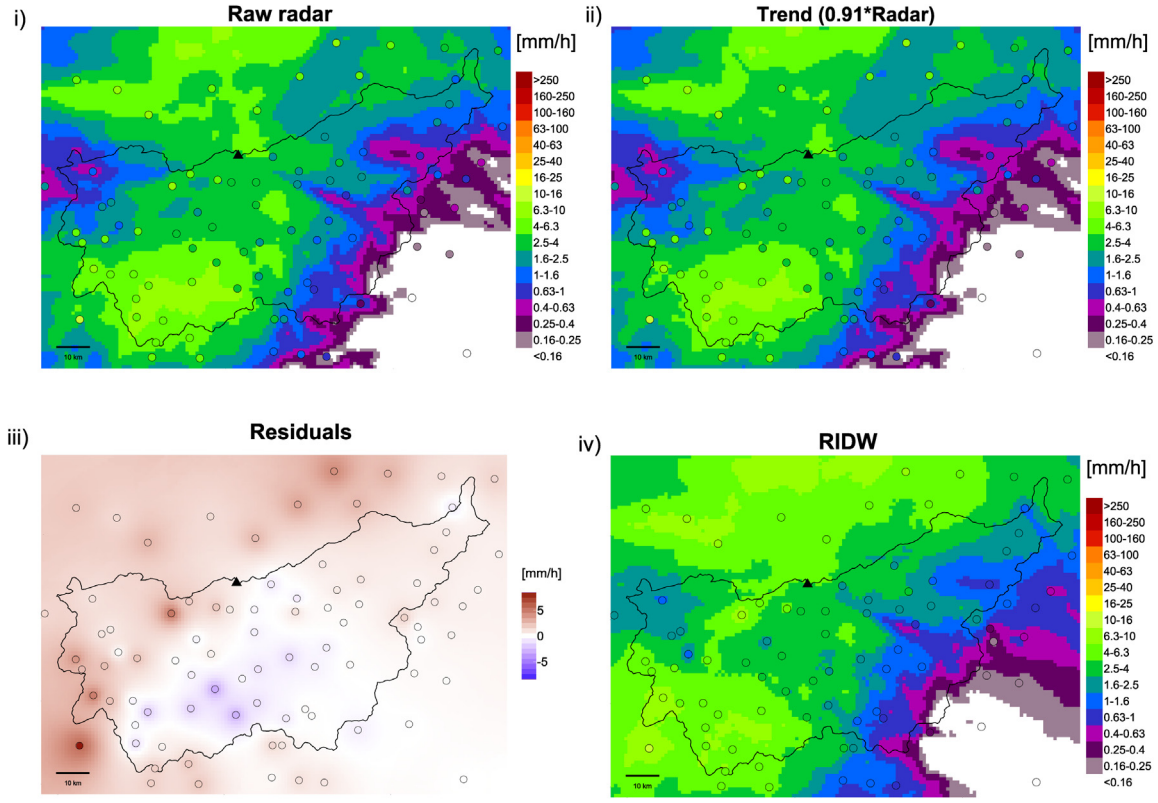


**Fig. 2.** Illustration of the different steps in RIDW: (i) Raw radar data; (ii) Trend obtained by multiplying the raw radar data by the regression coefficient (Eq. (7)); (iii) Residuals computed for each station and interpolated; (iv) Final product obtained by adding the trend (ii) and the interpolated residuals (iii). Circles represent rain gauge locations and filling colour the precipitation intensity observed at the station. The black triangle represents the radar of Pointe de la Plaine Morte. (Time step: 01-05-2015 2200 UTC + 1).

(c) the interpolation of the residuals, to explore for example a larger number of stations in the last step.

Eqs. (5)–(8) about trend and residuals computation remain valid for RK. The covariance of the residuals at the locations of observation is given by the *NxN* covariance matrix $\boldsymbol{C_{aa}}$:

$$\mathbf{C_{aa}} = \begin{pmatrix} \sigma_Z^2 & C_{12} & \cdots & C_{1N} \\ C_{21} & \sigma_Z^2 & \cdots & C_{2N} \\ \vdots & \vdots & \ddots & \vdots \\ C_{N2} & C_{N2} & \cdots & \sigma_Z^2 \end{pmatrix} \tag{10}$$

where each element $C_{ij}$ of the matrix is given by the covariance between the observation locations $i$ and $j$ and $\sigma_Z^2$ is the variance of the observations. Assuming a gaussian distribution of the residuals (discussed later in Section 3.3) and considering a constant zero mean and known variance, we use Simple kriging to spatialize the residuals. Considering the two conditions imposed by the kriging approach which are (i) an unbiased estimator and (ii) a minimal estimation variance, the following equation is obtained (Webster and Oliver, 2007):

$$\mathbf{C}_{aa}\lambda = \mathbf{c_a} \tag{11}$$

where $\mathbf{c_a}$ is the covariance vector between the locations of interpolation and the observation locations.

Resolution of the system given in Eq. (11) provides the weights for the linear kriging predictor used to compute residual values at the interpolation location $s_0$, given by the linear combination of the observations:

$$\hat{\epsilon}_{\mathrm{RK}}(s_0, t) = \sum_{i=1}^{N} \lambda_i \, \epsilon(\mathbf{s}, t) \tag{12}$$

which is then added to the trend $m_p(s_0, t)$ to get the expected value of the precipitation depth:

$$\hat{p}_{\mathrm{RK}}(s_0, t) = m_p(s_0, t) + \hat{\epsilon}_{\mathrm{RK}}(s_0, t) \tag{13}$$

$\forall\ s_0 \in D \subseteq \mathbb{R}^2$

Interpolation of the residual is done using a global neighborhood, that means all the points are used for the interpolation.

### 3.1.5. Regression co-kriging (RCK)

Based on the comparative analysis between the MeteoSwiss and MeteoGroup networks (see Section 2), the choice was made to explore a variant of Regression-kriging using co-kriging and hereafter referred to as Regression co-kriging (RCK). Co-kriging has the advantage of offering the possibility of considering more than one variable in the kriging interpolation.

Thus, the multivariate RCK variant allows considering different vectors of rain gauges. Instead of having only one vector of observations, vector $\boldsymbol{g}(t)$ of Eq. (1) is replaced by two vectors:

$$\mathbf{g_a}(t) = [g(s_{a,1}, t), g(s_{a,2}, t), \ldots, g(s_{a,N_a}, t)] \tag{14}$$

$$\mathbf{g_b}(t) = [g(s_{b,1}, t), g(s_{b,2}, t), \ldots, g(s_{b,N_b}, t)] \tag{15}$$

where the subscripts $a$ and $b$ refer to the primary (a) and secondary (b) networks and $N_a$ and $N_b$ are the number of available rain gauges in respectively the primary and the secondary networks over the period $t$.

Similarly, the radar precipitation estimates' vector of Eq. (4) is replaced by two vectors:

$$\mathbf{r_a}(t) = [r(s_{a,1}, t), r(s_{a,2}, t), \ldots, r(s_{a,N_a}, t)] \tag{16}$$

$$\mathbf{r_b}(t) = [r(s_{b,1}, t), r(s_{b,2}, t), \ldots, r(s_{b,N_b}, t)] \tag{17}$$

Statements about the trend and residuals computation of Eqs. (5)–(8) remain valid. The residuals are computed with the two equations:

$$\epsilon_a(\boldsymbol{s_a}, t) = g_a(\boldsymbol{s_a}, t) - a_a r_a(\boldsymbol{s_a}, t) \quad (18)$$

$$\epsilon_b(\boldsymbol{s_b}, t) = g_b(\boldsymbol{s_b}, t) - a_b r_b(\boldsymbol{s_b}, t) \quad (19)$$

where $a_a$ and $a_b$ are the multiplicative coefficients for the primary and secondary variables computed with a linear regression of the radar data on the rain gauge data. These two terms are the result of a linear regression computed for each of the corresponding subsets of data with respect to the corresponding radar data.

The consideration of two variables in RCK instead of one modifies Eq. (11) as follows (Myers, 1982):

$$\begin{pmatrix} \mathbf{C_{aa}} & \mathbf{C_{ab}} \\ \mathbf{C_{ba}} & \mathbf{C_{bb}} \end{pmatrix} \begin{pmatrix} \lambda_a \\ \lambda_b \end{pmatrix} = \begin{pmatrix} \mathbf{c_a} \\ \mathbf{c_b} \end{pmatrix} \quad (20)$$

where $\mathbf{c_a}$ and $\mathbf{c_b}$ are the covariance vectors of residuals between the unmonitored locations and the locations with observations and $\mathbf{C_{ab}}$ (respectively $\mathbf{C_{ba}}$) the cross-covariance matrix between the primary and secondary variables (respectively the secondary and primary variables). Consequently, the estimator equation is given by:

$$\hat{\epsilon}_{\mathrm{RCK}}(s_0, t) = \sum_{i=1}^{N_a} \lambda_{a,i}\, \epsilon_a(\boldsymbol{s_a}, t) + \sum_{i=1}^{N_b} \lambda_{b,i}\, \epsilon_b(\boldsymbol{s_b}, t) \quad (21)$$

before being added to the trend $m_p(s_0, t)$:

$$\hat{p}_{\mathrm{RCK}}(s_0, t) = m_p(s_0, t) + \hat{\epsilon}_{\mathrm{RCK}}(s_0, t) \quad \forall\, s_0 \in D \subseteq \mathbb{R}^2 \quad (22)$$

### 3.2. Variogram fitting for non-collocated networks

Computation of the weights vector $\lambda$ of Eq. (11) as well as $\lambda_a$ and $\lambda_b$ of Eq. (20) requires an estimate of the covariance matrices. Instead of computing the covariance, which is sensitive to sampling effects, kriging generally uses the concept of semivariogram (Matheron, 1971), which represents how the dissimilarity between pairs of points increases with increasing separation distance. The semivariogram, or simply variogram as called from now, is defined for the univariate case and expressed in terms of precipitation residuals by:

$$\gamma_a(h) = \frac{1}{2N(h)} \sum_{i=1}^{N(h)} (\epsilon(s_i) - \epsilon(s_i + h_i))^2 \quad \forall\, (s_i, s_i + h_i) \in D \subseteq \mathbb{R}^2 \;\mid\; h_i \in [h - b/2,\, h + b/2], \quad (23)$$

where $h$ is the distance lag between pairs of locations, $\gamma_a(h)$ the variogram value for distance lag $h$, $b$ the bin size (the width of the distance interval up to which point pairs are grouped for variogram computation), $h_i$ the distance separing a given pair of points, $N(h)$ the number of considered pairs of observations separated by distance $h$, $\epsilon_a(s_i)$ the residual value at location $s_i$ and $\epsilon(s_i + h_i)$ the residual value at location $s_i + h_i$ (Pebesma, 2014).

In the case of Regression kriging, one variogram is computed with Eq. (23) for each time step of computation. For the Regression co-kriging, two direct variogams (one for each variable) and one cross-variogram must be computed to define the so-called linear model of coregionalization (Webster and Oliver, 2007). For the computation of the cross-variogram, Eq. (23) must be generalized to two variables, identified by the subscript $a$ and $b$:

$$\gamma_{ab}(h) = \frac{1}{2N(h)} \sum_{i=1}^{N(h)} (\epsilon_a(s_i) - \epsilon_a(s_i + h_i))(\epsilon_b(s_i) - \epsilon_b(s_i + h_i)) \quad \forall\, (s_i, s_i + h_i) \in D \subseteq \mathbb{R}^2 \;\mid\; h_i \in [h - b/2,\, h + b/2] \quad (24)$$

where $\epsilon_b(s_i)$ is the residual value at location $s_i$ and $\epsilon_b(s_i + h_i)$ the residual value at location $s_i + h_i$.

However, Eq. (24) can be used only in case of collocated variables (observations for both variables are available for a sufficient number of given points). In the case of SMN and MG stations, this is not the case as stations are situated in different locations. Accordingly, one needs to work with so-called pseudo cross-variograms in which pairs of both variables are considered, as proposed by Pebesma (2014):

$$\gamma^*_{ab}(h) = \frac{1}{2N(h)} \sum_{i=1}^{N(h)} (\epsilon_a(s_i) - \epsilon_b(s_i + h_i))^2 \quad \forall\, (s_i, s_i + h_i) \in D \subseteq \mathbb{R}^2 \;\mid\; h_i \in [h - b/2,\, h + b/2] \quad (25)$$

where $\gamma^*_{ab}(h)$ is the pseudo cross-variogram value for distance lag $h$ considering variables $a$ and $b$.

The equivalence between variogram and covariance is defined for second-order stationary processes (for which the variogram is always bounded), as follows (Webster and Oliver, 2007):

$$\gamma(h) = C(0) - C(h) \quad (26)$$

where $\gamma(h)$ is the variogram value for a distance $h$, $C(0)$ is the covariance at $h = 0$ and $C(h)$ the covariance at distance $h$. If the variogram is bounded by a sill, the value of $C(0)$ is equal to the total sill value.

In the present study, the variogram models have been fitted using the package 'gstat' (Pebesma and Graeler, 2017), within the software R (R Core Team, 2016). The empirical variogram has been fitted with a spherical variogram model (Schuurmans et al., 2007):

$$\gamma(h) = \begin{cases} 0 & \text{if } h = 0, \\ K_0 + K\left(\frac{3h}{2\alpha} - \frac{h^3}{2\alpha^3}\right) & \text{if } 0 < h \leqslant \alpha, \\ K_0 + K & \text{if } h > \alpha. \end{cases} \quad (27)$$

in which $K_0$ is the nugget value, $K$ the partial sill, $\alpha$ the range (distance within which measures are considered correlated).

The implemented code explores different values of bin size until a valid variogram model can be fitted. The routine also tries to obtain a low nugget-to-sill ratio by gradually increasing a success threshold: 100 iterations are first attempted with a threshold value of 0.1. If none of the obtained valid models has a nugget-to-sill ratio lower than the threshold, the threshold is increased by 0.1 until 0.9 with each time 100 iterations. In case of failure with the highest threshold value, the last valid variogram of previous time steps is considered.

Anisotropy of the variogram (different spatial variability in different directions) has not been explored in this work. This choice is justified by the use of the radar data, in which spatial variability of the precipitation fields is assumed to be contained and therefore considered in the interpolation process.

### 3.3. Transformation

Precipitation is inherently heteroscedastic (the variance is not constant over the domain) and has a skewed distribution, which is in contradiction with basic assumptions of classical geostatistics which assumes a gaussian distribution and stationarity of the mean and spatial covariance (Erdin et al., 2012). Therefore, several methods have been explored in the literature to transform the data before their interpolation (Sideris et al., 2014a; Erdin et al., 2012; Schuurmans et al., 2007) and it has been shown that quantitative improvements is dependent on temporal and spatial variability (Cecinati et al., 2017b). The process of applying kriging to data transformed into a more gaussian distribution is generally named trans-gaussian kriging.

In the case of the two methods employing kriging in this paper, namely regression kriging (RK) and regression co-kriging (RCK), interpolation is not done directly on the precipitation observations but on the residuals (see Section 3.1), to which the gaussianity issue therefore applies. A transformation is applied to both the rain gauge and the radar data to translate them into a more gaussian distribution, with the objective of getting better gaussianity in the residuals. In this paper, we use for both RK (3.1.4) and RCK (3.1.5) methods a square-root transformation of the data (Sideris et al., 2014a). Analysis of the residuals distribution has shown that this transformation tends to increase overall

the gaussianity of the residuals, even though the effect is somewhat limited and for few time steps even negative. In analysing the effect of such data transformation on precipitation interpolation, Erdin et al. (2012) reported "only small effects of transformation for the point estimates" but mentioned that "transformation improved the reliability of the probabilistic estimates substantially". The corresponding gain of introducing such transformation scheme is disscussed in Section 4.2.2.

The advantage of the square-root transformation is the possibility of analytical back-transformation of the mean and the variance (Sideris et al., 2014a), given by:

$$\mathrm{E}[Y^2] = \mu_Y^2 + \sigma_Y^2 \tag{28}$$

and,

$$\mathrm{Var}[Y^2] = 4\mu_Y^2\sigma_Y^2 + 2\sigma_Y^4 \tag{29}$$

where $\mu_Y$ is the mean and $\sigma_Y$ the standard deviation of the square-root-transformed kriging prediction at a certain location, whereas $\mathrm{E}[Y^2]$ represents the expected value of the back-transformed random variable, or, in other words, the final prediction, and $\mathrm{Var}[Y^2]$ the related variance. However, Eq. (28) is composed of two positive terms (both are squared values) with the variance ($\sigma_Y^2$) being positive and reaching the sample variance of the (transformed) residuals at estimation locations situated at a distance from the nearest observation higher than the variogram model range (Eq. 27). Thereby, the back-transformed estimation would never provide zero precipitation estimates apart from rain gauge locations (where estimation variance is minimum). In the work of Sideris et al. (2014a), this problem is addressed by correcting the interpolated field and assigning zero precipitation to locations where the radar does not show any precipitation (I. Sideris, personal communication, May 30, 2017). The methodology proposed here overcomes this issue by weighting the variance term of Eq. (28) with the predicted precipitation:

$$\sigma_Y^{*2} = \frac{\mu_Y^2}{\tau}\sigma_Y^2 \tag{30}$$

where $\tau$ is a precipitation intensity threshold below which the variance is weighted and $\sigma_Y^{*2}$ is the variance effectively added in Eq. (28) instead of $\sigma_Y^2$, which gives:

$$\mathrm{E}[Y^2]^* = \mu_Y^2 + \sigma_Y^{*2} \tag{31}$$

where $\mathrm{E}[Y^2]^*$ represents the expected value of the back-transformed random variable considering the modified estimation variance. The value for $\tau$ has been fixed to 0.5 mm/h after initial tests. The impact of applying the transformation or not is discussed in Section 4.2.2.

### 3.4. Skill scores and cross-validation

The performance analysis is based on the leave-one-out approach: the precipitation is estimated at a rain gauge location using all observations except the one corresponding to the interpolation location. The procedure is undertaken on an hourly basis for each location and for each of the methods. The quality of the point estimates is then assessed over all locations for each time step using following skill scores:

1. Bias: Systematic errors are assessed with the bias indicator:

$$\mathrm{Bias}(t) := 10\log_{10}\frac{\sum_{i=1}^{N}\hat{g}_i(t)}{\sum_{i=1}^{N}g_i(t)} \tag{32}$$

where $\hat{g}_i(t)$ refers to the estimated value for a given location and a given time step, $g_i(t)$ to the observed value and $N$ to the number of considered locations. As a result of the logarithmic scale used in Eq. (32), the bias is expressed in decibel (dB). For each event, the overall bias is averaged over the entire period and the entire spatial extent. The bias has been computed only for hourly time steps during which the mean precipitation over the MeteoSwiss stations was higher than 0.5 mm/h. This avoids values at the denominator close to 0, resulting in exaggeratedly high bias values.

2. MAD: The median absolute deviation (MAD), provides the median of the absolute value of the difference between estimated and observed values (Sideris et al., 2014a):

$$\mathrm{MAD}(t) := \mathrm{median}(|\hat{g}_i(t) - g_i(t)|) \tag{33}$$

3. RMSE: The Root mean square error is the most common parameter used in verification (Goudenhoofdt and Delobbe, 2009). It represents the standard deviation of the differences between predicted and observed values:

$$\mathrm{RMSE}(t) := \sqrt{\frac{\sum_{i=1}^{N}(\hat{g}_i(t) - g_i(t))^2}{N}} \tag{34}$$

4. MRTE: The mean-root-transformed error (Erdin et al., 2012), mitigates the dominant influence of errors at large precipitation amounts as compared to RMSE:

$$\mathrm{MRTE}(t) := \frac{1}{N}\sum_{i=1}^{N}(\sqrt{\hat{g}_i(t)} - \sqrt{g_i(t)})^2 \tag{35}$$

5. Scatter: The scatter is a measure of the spread of the ratio between estimated and measured values. It is based on the cumulative error distribution function of these ratios, expressed in decibel (Germann et al., 2006; Schiemann et al., 2011):

$$\mathrm{Scatter} := \frac{1}{2}(\xi_{84} - \xi_{16}) \tag{36}$$

where $\xi_{16}$ and $\xi_{84}$ represent the 16% and the 84% percentiles of the cumulative error distribution function. Only pairs of points for which both estimated and observed values where higher than 0.5 mm/h were considered for the computation of the scatter.

### 3.5. Methodology application

For the IDW method, a value of 2 (common default value) is given to the power coefficient $\beta$ (Eq. 3) and the research radius is fixed to 50 km. For the methods including a regression of the radar data, the regression has been computed only on stations located within the basin.

For the methods considering a single rain gauge network (IDW, RIDW and RK), the primary variable (SMN) data are considered. For the RCK method, both primary (SMN) and secondary (MG) variables data are used.

Variograms fitting with an insufficient number of points can lead to ill-defined variogram. For the RK method, a minimum of 5 stations with a precipitation of at least 0.5 mm/h is set as condition. For the RCK method, the condition is set to 5 stations exceeding the same precipitation threshold value for each variable. When the condition is not satisfied, the last previously computed valid variogram is used. The condition being generally not satisfied at the beginning of an event, an initial variogram must preliminarily be computed over an arbitrarily chosen time step during the event with sufficient stations exceeding the threshold.

In addition, for both the RK and RCK methods, the model fitting has been constrained to a maximum range of 50 km. This value has been defined based on visual variogram analysis and allows to constrain the model for experimental variograms that do not show a clear upper bound.

## 4. Results

The five methods presented in Section 3 and listed in Table 5 have been applied to the four events presented in Section 2.5.2. For all the

**Table 5**
Analyzed methods and corresponding used data. For methods abbreviations, see Table 3.

| Application | Radar | Primary variable | Secondary variable |
|---|---|---|---|
| Radar | Yes | – | – |
| IDW(SMN) | No | SMN | – |
| RIDW(SMN) | Yes | SMN | – |
| RK(SMN) | Yes | SMN | – |
| RCK(SMN,MG) | Yes | SMN | MG |

five methods, the interpolation has been computed over a grid with a resolution corresponding to the one of the raw radar data (1 km$^2$ per pixel).

For the cross-validation, the computation was based on the locations of the SMN rain gauges within the basin, even if more stations such as MG stations were used for the interpolation, to ensure a constant comparison basis for all methods. It is worth noting here that no direct comparison has been possible within this study with the *CombiPrecip* product of MeteoSwiss, as no leave-one-out computation was possible on the delivered *CombiPrecip* product.

The performance of the different methods is first discussed based on the cross-validation approach, including a discussion of the performance before the installation of the new weather radar in 2014. Results of the variogram fitting and the effect of data transformation are then presented. The last section discusses the effect of additional networks.

### 4.1. Methods performance analysis

In order to assess the performance of the different methods, the presented performance indicators have been computed for the four events 1 to 4 (Table 2). For each performance indicator (Table 4), hourly values were averaged over each event. Results are given in Fig. 3. The cumulative volume over the events, considering all the pixels located within the basin, is also presented (dashed line border).

The estimation method considering only raw radar data (Radar) clearly shows the weakest performance. Particularly in terms of bias, which confirms the need of bias correction of the raw radar data with a regression using rain gauges. This observation is strengthened by the total volume that differs substantially from the other methods for part of the events. Overall, the RCK method provides the best performance. This is the case for the MRTE indicator for which the RCK method provides the best value over all four events. In terms of absolute bias, RCK outperforms for all the events the RK method but for some events, other methods such as IDW perform better than RCK. Furthermore, the results are not clear for all the indicators. For example for event 1, RMSE and Scatter values are comparable for RCK and IDW. It is worth to recall here that the station density within the basin is particularly high, which allows IDW to reach already good performances. It must also be pointed out that IDW has been applied with the default value of 2 for the exponent $\beta$ of Eq. (2). Adjustment of this parameter could improve the performance of the IDW method.

For a finer analysis, Fig. 4 presents hourly values for the four performance indicators computed at each time step, for the reference IDW method and the RCK method. Scatter is not shown here as it is computed directly over the events. Results for the bias show how reactive the indicator can be, with a strong negative value for the RCK method on 2 May 2015 at 16:00. However, this corresponds to the beginning of the second front and only few stations already observed precipitation, in which case one single important cross-validation error can strongly affect the hourly indicator value. It must also be noted that such single negative (respectively positive) values can compensate for an overall positive (respectively negative) bias value and lead to an improvement in the overall value. This is one of the limitation of the bias indicator.

Regarding the three other indicators, all strictly positive by definition, it is interesting to note the varying difference between the two methods over the three fronts: whereas there is only a small gain of RCK over IDW over the first front, it increases over the second and third front, in particular for the MRTE indicator. When analyzing the different fronts, it appears that over the third one, only the north-western part of the basin is covered by the precipitation (Fig. 5). The gain of integrating the radar information is here clearly visible, with the IDW

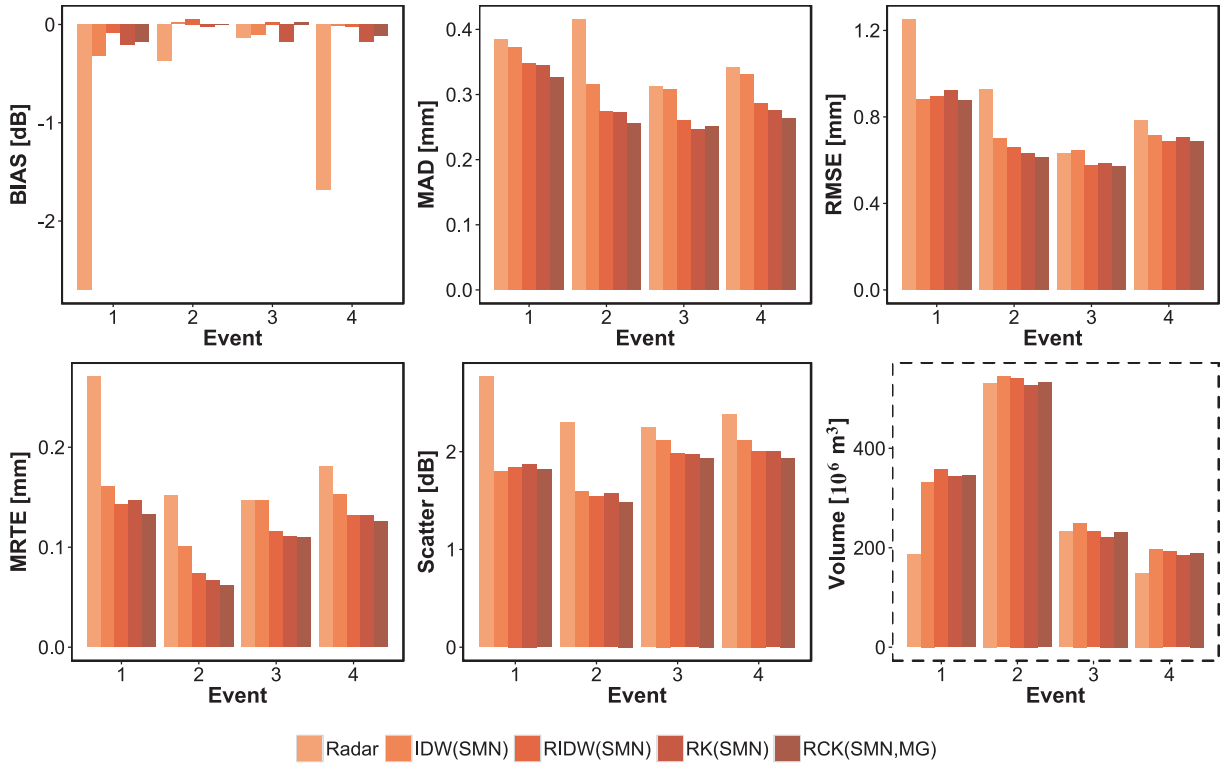


**Fig. 3.** Event-averaged performance indicator values and cumulative volume over the entire basin (dashed line border) over the 4 events.

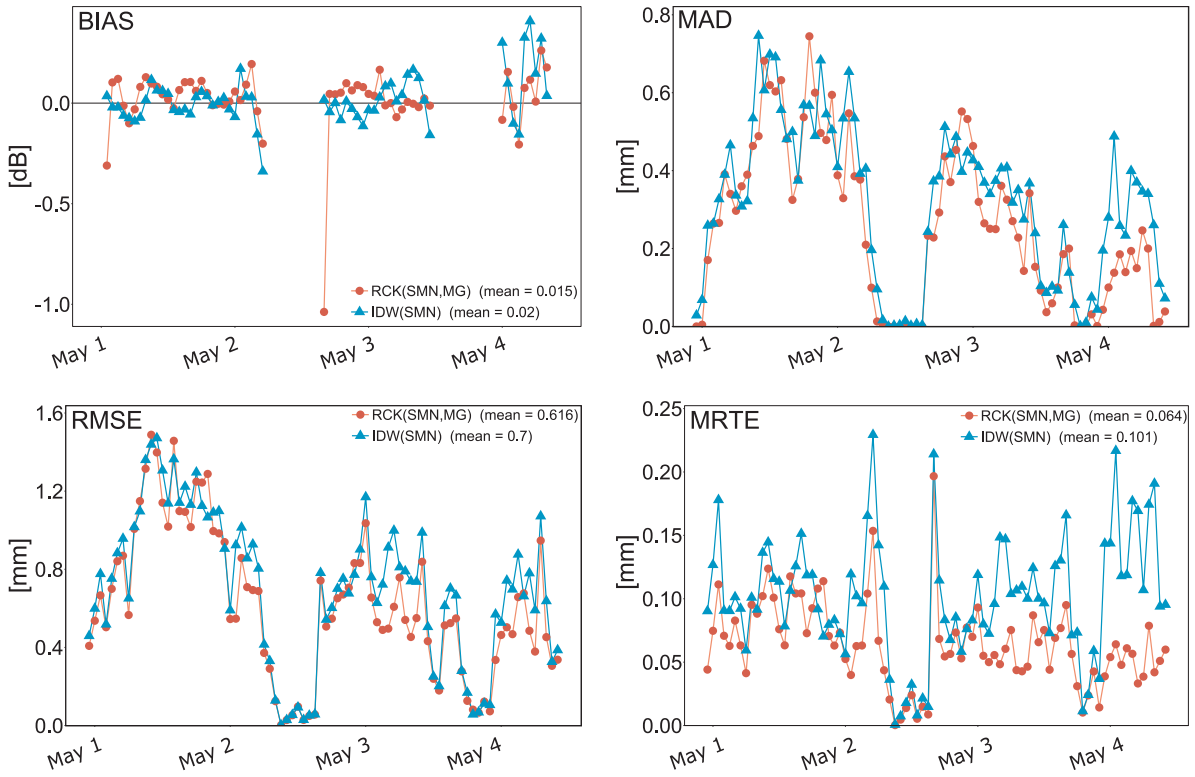


**Fig. 4.** Hourly values of performance indicators for IDW(SMN) and RCK(SMN,MG) over event 2 (May 2015).

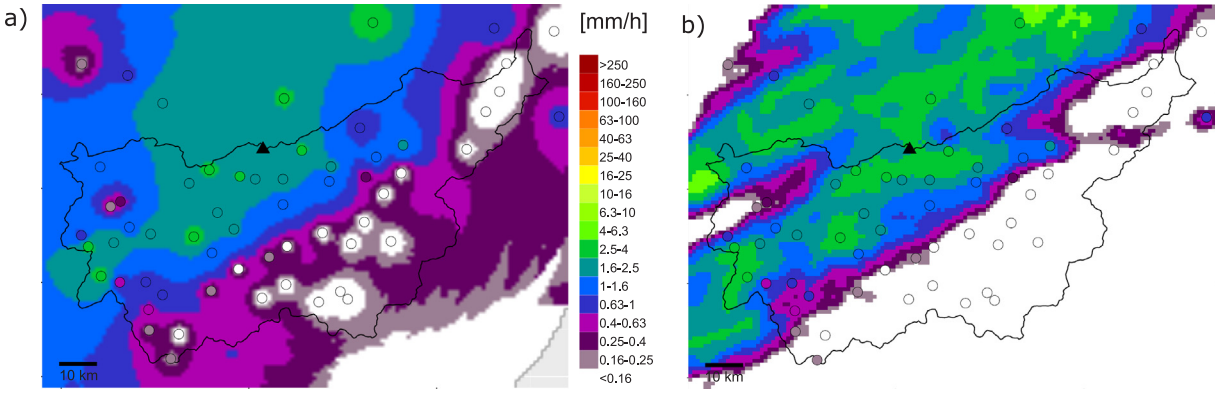


**Fig. 5.** Hourly interpolated precipitation using (a) IDW(SMN) and (b) RCK(SMN,MG) on 04-05-2015 0100 UTC + 1. Circles represent rain gauges' locations and filling colour the intensity observed at the station. The black triangle represents the radar of Pointe de la Plaine Morte.

method not being able to reproduce the sharp gradient cutting the basin in two parts. Figs. S.5 to S.10 (Supp. Mat.) show the same indicators for the 6 other events.

When analyzing the cross-validation errors of event 1, it appeared that the station Col du Grand St-Bernard (GSB) resulted almost systematically (over the entire event) in high cross-validation errors, with both IDW and RCK methods not being able to correctly reproduce the observed precipitation, despite using the radar information in the RCK method. When looking at the total precipitation over the event for both methods, the GSB station is also very well visible at the south-western corner of the basin (Fig. 6). The high difference between the rain gauge values and the bias-corrected radar data only at this station suggested to further investigate this particularity. Interestingly, this station, located at an elevation of 2472 m asl., had already been pointed out in a precedent analysis (Erdin et al., 2012), in which the station was reported to suffer of "several known measurement problems (shielding, wind exposure, and drifting snow)". And with a snow limit varying between 1000 and 2000 m asl. over the event 1, the GSB station only measured solid precipitation.

To investigate the impact of the station over the global performance over the event, the interpolation has been recomputed by totally excluding the GSB station. Fig. 7 shows the result for the two methods, both with and without considering the GSB station. Results show that all indicators are improved when removing the station. In particular for RMSE and MRTE, the difference is non-negligible. This example shows well how considering as truth the data from the rain gauges can lead to incoherence or errors in the interpolation result.

The analysis carried out over events 1 to 4 considered radar data including the new radar of Pointe de la Plaine Morte. In order to assess the quality of the Swiss-wide radar product over the studied basin before the installation of this new radar, performances over the three events A, B and C are presented in Fig. 8. The performance gain of RCK over IDW for the three events is higher than for events 1 to 4. This is probably partly explained by the number of rain gauges available over the three events: only 28 and 40 SMN stations for 2012 (event A) and 2013 (event B) whereas at least 52 stations were available for the events

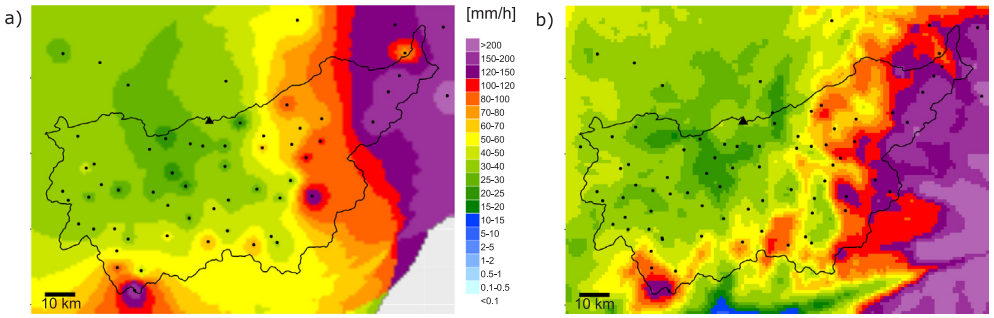


**Fig. 6.** Comparison of total precipitation over event 1 (04-11-2014 0800 to 06-11-2014 0400 UTC + 1) for (a) IDW(SMN) and (b) RCK(SMN,MG). The black points represent the locations of the considered rain gauges. The black triangle represents the radar of Pointe de la Plaine Morte. The gray back-ground on the bottom-right corner of (a) results from the absence of data within the research radius (50 km) of these pixels.

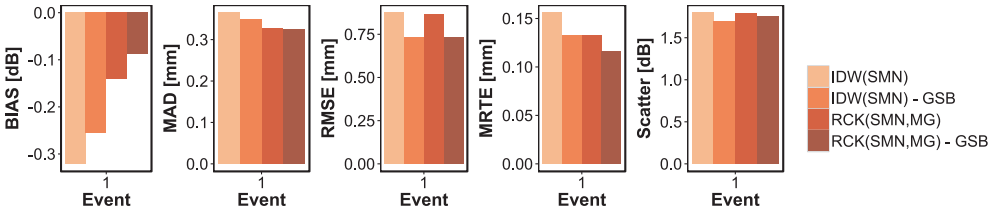


**Fig. 7.** Performance indicators over event 1 with exclusion of Col du Grand St-Bernard (GSB) station.

1 to 4. The lower station density reduces the performance of IDW and thereby increases the relative gain of RCK over IDW.

The performance of the RCK method over the three analyzed events excluding Pointe de la Plaine Morte radar data suggests that this method provides clearly better results than IDW for the studied basin even before the installation of the new weather radar. This is an important result in the perspective of computing precipitation fields for hydrological modelling with data requirement over relatively long time periods, as it shows that even with an Alpine topography like the one in the studied basin, radar data seem to be usable even without a weather radar located within the basin.

### 4.2. Variogram and data transformation analysis

Performance of the variogram model fitting for the results presented in Section 4.1 are presented hereafter, before analyzing the effect of data transformation looking at the RCK method.

#### 4.2.1. Variogram fitting results

Good fitting of the variogram is essential to obtain a reliable interpolation. The implemented solution resulted in few time steps (0.5%) without valid variogram fitting. This considers only the time steps with enough stations reporting sufficient precipitation as defined in Section 3.5. The percentage of time steps with insufficient stations is considerably high: 7.4% for the RK method and 31.7% for the RCK method of the time steps over the four events 1 to 4. These time steps generally correspond to the lower intensity phase of the events. For all these time steps (both failure and insufficient stations), the previously computed last valid variogram was used instead.

Fig. 9 shows four direct variograms for the RK method over event 3. The differences in bin size are well visible: the fewer points are visible on a sample variogram, the more points were grouped together and averaged to compute each point of the experimental variogram. Fig. 10 gives an example of the linear model of coregionalization, composed of two direct variograms (SMN and MG) and one pseudo cross-variogram (SMN vs. MG), all three fitted simultaneously. The higher variability observed in the MG direct variogram tends to be a common behavior within this study. This difference cannot be directly attributed to a difference in the quality of the MG sensors, as these stations are also much less numerous, with only 23 MG stations for 52 SMN stations over the chosen event, enhancing the issue of limited number of wet stations for the MG network.

In addition, if most of the fitted models describe well the experimental variogram, for some times steps, a manual fitting would probably have led to more appropriate fittings.

#### 4.2.2. Effect of data transformation

The RCK method has been applied to events 1 to 4, both with and without transformation (Fig. 11). The bias is considerably improved for two of the four considered events when applying the discussed square-root transformation (Eq. 31). For the MRTE, a gain is observed for all events. For the other indicators, the difference is less important and more variable, for example for the MAD, for which loss and gain are observed; for the Scatter, the tendency is slightly negative, probably due to the back-transformation process.

These results are coherent with the conclusions of Erdin et al. (2012), who reported only “small effects of the transformation” on the point estimates, but reported a higher reliability of the estimates when comparing “each gauge measurement against the probability function of the corresponding cross-validation probabilistic estimate”. Further

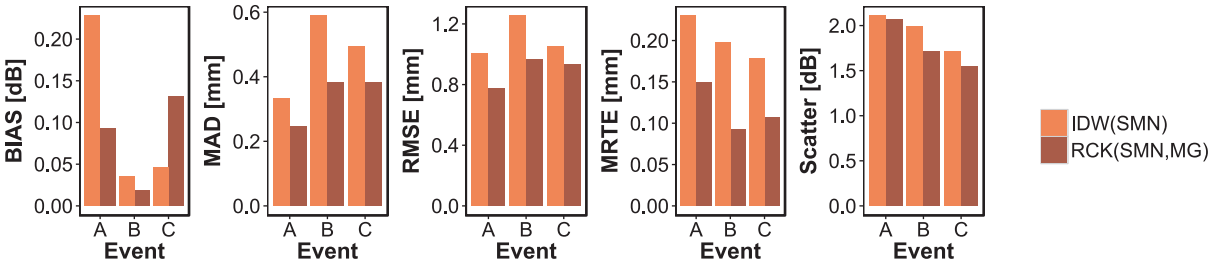


**Fig. 8.** Performance indicators for the method IDW using SMN data and the RCK method using SMN (primary) and MG (secondary) data over the 3 events without data for the radar of Pointe de la Plaine Morte.

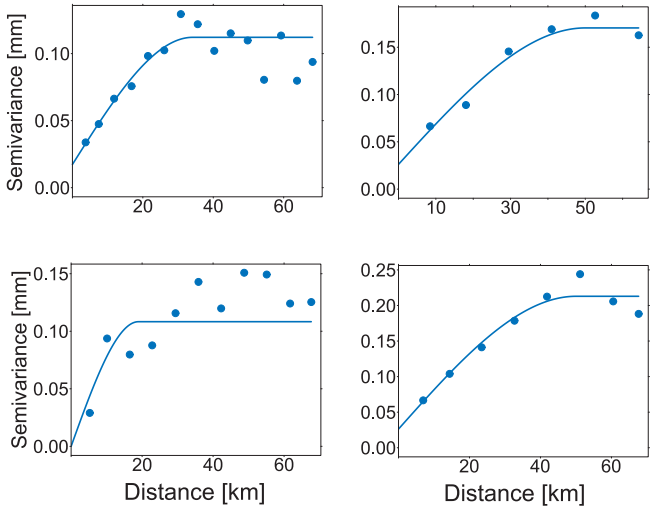


**Fig. 9.** Sample of the variogram and automatically fitted models for the first four hours of event 3 (January 2016).

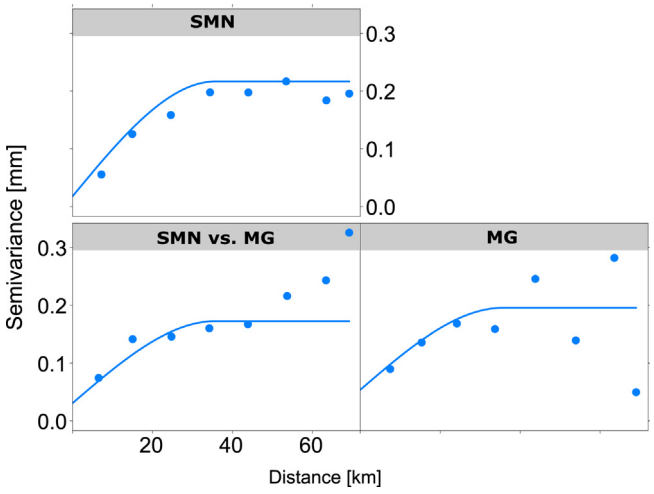


**Fig. 10.** Example of linear model of coregionalization composed of two direct variograms and one pseudo cross-variogram (bottom left) using SMN as primary variable and MG as secondary variable (01-05-2015 2200 UTC + 1).

improvements in the transformation could be explored, not only on the power coefficient of the transformation, but also on the back-transformation process. Based on the obtained results, applying the proposed transformation is recommended.

### 4.3. Effect of additional networks

In the results presented in Section 4.1, the MG data have been used only in the RCK method as secondary variable. Combination of SMN and MG data as a unique set of data is discussed hereafter. Fig. 12 presents the performance indicators for the IDW, RIDW and RK methods, each time considering first SMN data only and then combining SMN and MG data, considering them together as one single variable (Table 6). Results of RCK using SMN data as primary variable and MG as secondary variable are also presented.

For all indicators except the bias, considering MG data directly with SMN data as one single variable tended to improve the performance of the methods as compared to use only SMN data, which can be explained by the additional local information introduced by the MG stations. Performances were in some cases even slightly better than for RCK in which both variables are considered separately. However, and as expected from the data analysis presented in Section 2 (Study area and data), this joint use of SMN and MG data resulted in negative biases. This effect is well visible in particular for events 3 and 4 (Fig. 12), where values exceeded −0.6 dB corresponding to a negative bias of about −13%. Consequently, this bias issue suggests to consider both variables only with methods accounting for this deviation, that means in the present case the RCK method.

The present study also aimed at providing a preliminary analysis of integrating stations from surrounding areas. This is justified by the need for accurate information in terms of precipitation estimates for real-time hydro-meteorological monitoring and forecasting. Fig. 13 shows for a time step of event 2 the interpolation results of RCK, using only SMN and MG data compared to the results obtained with integrating the data from all surroundings additional networks. With the additional stations, precipitation estimates are for example increased over the Aosta region south of the studied basin (see Fig. 13c).

For a more quantitative assessment, Fig. 14 gives the corresponding performance indicators, including different combinations of primary and secondary variables for the precipitation interpolation. The additional data have however not been used for the linear regression computation nor for the variogram fitting. This was motivated respectively to ensure an optimal radar regression over the studied basin and to reduce the risk of inconsistencies in the variogram model fitting, sensitive to discrepancies in even only one or two stations, potentially affecting the entire interpolation of a given time step.

The results show that adding additional networks has a limited effect. Bias tends to be the most reactive indicator, even tough differences are small. For the other indicators, as well as for the total precipitated volume, differences can be considered as limited, and it is difficult to define if it is rather a gain or a loss in terms of performance.

For some time steps, some stations of the additional networks reported no precipitation whereas the radar reported heavy precipitation, suggesting some possible quality issues. For operational purposes, the quality of these additional networks should be further investigated.

## 5. Discussion

The performance analysis used in this paper, based on leave-one-out cross-validation, did not allow a direct comparison with outputs of previous works, for example with the *CombiPrecip* product as described in Sideris et al. (2014a). In fact, the stations used in the cross-validation evaluation are used in the computation of the product, thus no comparison was possible. However, visual analysis of the interpolated precipitation fields revealed that the spatial patterns were very similar for a very large fraction of the time steps. Integration of the discussed interpolated precipitation fields into a hydrological model could allow a quantitative comparison between the products from a hydrological point of view. Furthermore, the analysis was carried out over the set of recent most heavy precipitation events, which were not evenly spread through all seasons, with events 1 to 4 (period 2014–2017) occurring from fall to spring and with events A to C (period 2012–2014) only in summer. This could have an impact on the analysis but should not modify the general conclusions from the comparison between methods.

The choice of performance indicators can also slightly modify the results of the analysis. For example, we decided to work with a bias indicator based on a ratio between estimated and observed values, indicator also used by several other authors (Sideris et al., 2014a; Goudenhoofdt and Delobbe, 2009). However, alternative versions exist, based for example on a differential bias (Cecinati et al., 2017b), less sensitive to small denominators.

Two aspects of the presented precipitation interpolation deserve further discussion, namely the integration of different rain gauge networks and remaining challenges, due mainly to radar visibility.

Regarding the integration of the data from the private MeteoGroup (MG) raingauges, it is important to point out here that their added value is probably somewhat underestimated in the presented results. In fact,

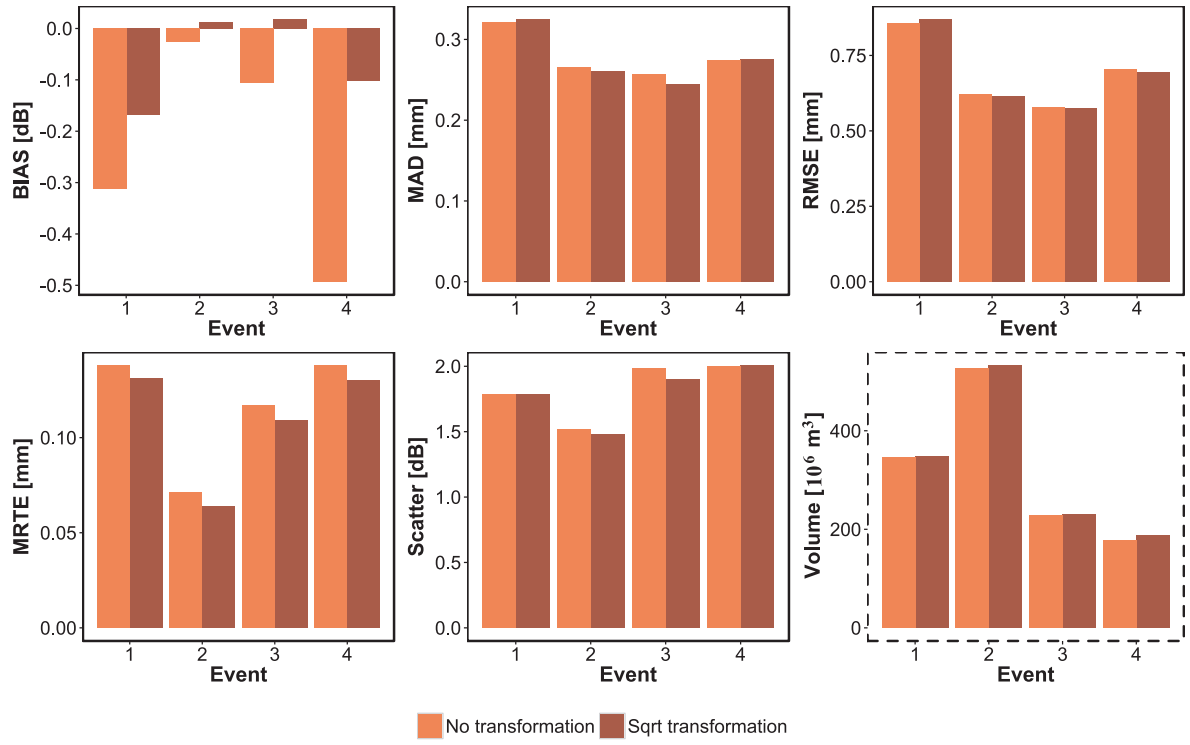


**Fig. 11.** Assessment of transforming or not the data when using the RCK(SMN,MG) method.

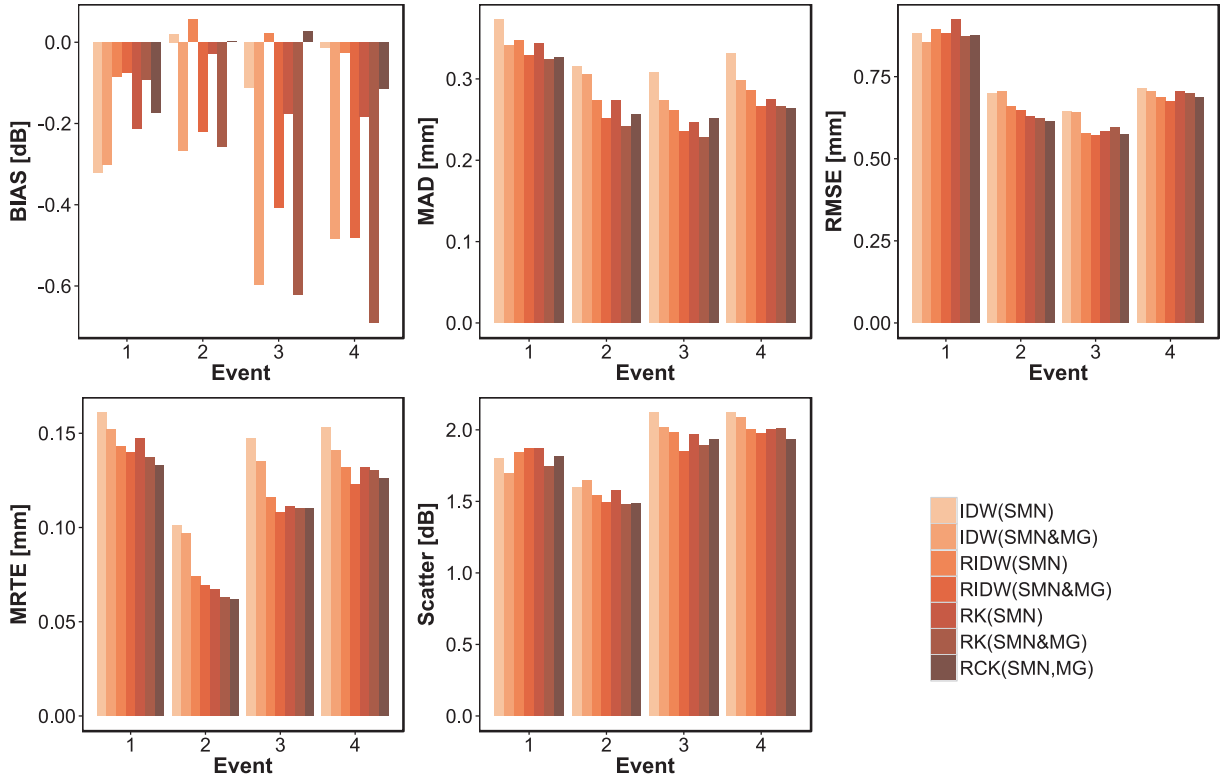


**Fig. 12.** Performance indicators over the 4 events, exploring combination of SMN and MG as primary variable for IDW, RIDW and RK methods.

their contribution to the overall interpolation quality is analyzed only via cross-validation applied to the MeteoSwiss (SMN) stations. This cross-validation does probably not show a complete picture of the contribution brought by the MG stations as (i) the MG stations have been selected to complete the SMN network in areas without SMN stations and (ii) the MG stations contribute to the final interpolated precipitation field mostly in their immediate vicinity.

As expected, including the radar data as external drift considerably improved the precipitation interpolation for all tested methods. However, any radar data set in a comparably complex area is highly likely to suffer from several quality issues such as radar beam shielding by mountain peaks located in close vicinity of the radars. For our case

**Table 6**
List of methods and data used for analysing the combination of SMN and MG data as a unique variable. For methods abbreviations, see Table Table 3.

| Application | Radar | Primary variable | Secondary variable |
|---|---|---|---|
| IDW(SMN) | No | SMN | – |
| IDW(SMN&MG) | No | SMN + MG | – |
| RIDW(SMN) | Yes | SMN | – |
| RIDW(SMN&MG) | Yes | SMN + MG | – |
| RK(SMN) | Yes | SMN | – |
| RK(SMN&MG) | Yes | SMN + MG | – |
| RCK(SMN,MG) | Yes | SMN | MG |

**Table 7**
Table of variables.

| Variable | Description |
|---|---|
| $a$ | Regression coefficient for trend computation |
| $b$ | Bin size for variogram computation |
| $C(h)$ | Covariance at distance h |
| $\mathbf{c_a}$ | Covariance vector between the location of interpolation and the monitored locations of variable A |
| $\mathbf{C_{aa}}$ | Covariance matrix between the residuals of variable A |
| $\mathbf{C_{bb}}$ | Covariance matrix between the residuals of variable B |
| $\mathbf{C_{ab}}$ | Cross-covariance matrix between the residuals of variable A to the residuals of variable B |
| $\mathbf{C_{ba}}$ | Cross-covariance matrix between the residuals of variable B to the residuals of variable A |
| $C_{ij}$ | Covariance between the residuals at locations i and j |
| $d$ | Distance separating two locations |
| $D$ | Spatial domain |
| $g$ | Rain gauge observation |
| $h$ | Distance lag between pairs of locations |
| $K_0$ | Nugget value |
| $K$ | Partial sill |
| $m$ | Trend component |
| $N$ | Number of available rain gauge measurements |
| $p$ | Precipitation depth |
| $r$ | Radar estimate |
| $s$ | Spatial coordinates |
| $\mathbf{s}$ | Spatial coordinates vector |
| $s_0$ | Spatial coordinates of interpolation location |
| $t$ | Period of time |
| $T$ | Temporal domain |
| $x$ | x coordinate |
| $y$ | y coordinate |
| $Y$ | Square-root-transformed random variable |
| $Y^2$ | Back-transformed random variable |
| $Z$ | Random variable |
| $\alpha$ | Variogram model range |
| $\beta$ | Power coefficient for the IDW method |
| $\epsilon$ | Residual component: observation - trend component |
| $\gamma(h)$ | Variogram model |
| $\gamma_a(h)$ | Univariate variogram |
| $\gamma_{ab}(h)$ | Cross-variogram |
| $\gamma^*_{ab}(h)$ | Pseudo cross-variogram |
| $\lambda$ | Interpolation weights |
| $\mu_Y$ | Mean of the square-root-transformed kriging prediction |
| $\rho$ | Research radius |
| $\sigma_Y$ | Standard deviation of the square-root-transformed kriging prediction |
| $\sigma^2_Z$ | Variance of the observations |
| $\tau$ | Precipitation intensity threshold for computation of variance to add in the back-transformation |

study, the Mont Bonvin (2994 m asl.), located two kilometers south-east of the radar of Pointe de la Plaine Morte (2926 m asl.), creates such a blind zone due to radar shielding in south-eastern direction from the radar location (visible in Fig. 15). In this area, precipitation is highly likely to be underestimated by the radar. This effect remains visible in the final estimation method retained here (RCK on the radar residuals with SMN as primary and MG as secondary variable) and is visible on Fig. 13. A similar effect can be seen on Fig. 6(b) for a second radar, the Monte Lema radar (south-east of the case study basin, see Fig. S.2 in Supp. Mat.). In fact, before the installation of the new radar at Pointe de la Plaine Morte, such shielding beams were already common over the studied basin as illustrated in the Supplementary Material (Figs. S.3 and S.4).

The radar network configuration in terms of installed devices is supposed to not evolve in the near future. The most promising directions to further improve precipitation interpolation under the current configuration are, thus, the following:

(i) Better accounting for radar shielding effects; the replacement by MeteoSwiss of their radar precipitation estimates product, used for the present study, by a new version, optimized for the new network configuration with 5 weather radars, will certainly contribute positively to this issue. Further investigations could e.g. consist in developing a raster of radar data quality based on the visibility of the weather radars or by analyzing the annual radar precipitation estimates. Such a method to account for radar quality should also consider temporal variations of the radar network configuration resulting from temporary inactivity of individual weather radars (due e.g. to technical failures or scheduled maintenance);
(ii) Improvement of the regression of the radar data on the rain gauge data, e.g. by including a second coefficient in the linear regression (Eq. 7), by developing a more local regression method that could account explicitly for summer convective precipitation or by integrating other covariates (e.g. topography).

In addition, latest developments in the field of hydrometeor type classification from radar data (Grazioli et al., 2015), might open up new perspectives on precipitation-radar data integration for mixed snow and rain events in the near future, as well as higher quality radar precipitation estimates during snow fall.

A final point worth mentioning is the potential integration of secondary rain gauge networks composed of non-heated stations that can only observe liquid precipitation, such as the Agrometeo network (Agroscope, 2017) or the IMIS network (SLF, 2017) to further increase the density of rain observation stations. This is readily possible with the retained interpolation methodology and could potentially reduce the precipitation estimation error during rainfall events. However, 75.1 percent of the studied area lies above 1500 m asl., where precipitation occurs regularly in the form of snow between November and March (Marty, 2008). In addition, with the high density of higher quality data already available, it is not sure that this would improve the performance.

## 6. Conclusion

This paper proposes a new method named Regression co-kriging for spatial interpolation of observed precipitation from two non-collocated rain gauge networks of different quality with radar data. Compared to the precipitation fields routinely produced in real-time by the Swiss national meteorological service MeteoSwiss (Sideris et al., 2014a) based on the observed precipitation data from their SwissMetNet (SMN) network, the final interpolation method retained here, additionally integrates data from the network of the private company MeteoGroup Switzerland AG (MG).

The performance of the interpolated precipitation fields is assessed for four events over a Swiss Alpine region, the Upper Rhône River basin, using inverse distance weighting applied directly to the rain gauge observations as baseline scenario. A series of well-established precipitation interpolation methods are tested, including methods that use (i) the radar data as an external drift to compute an overall precipitation trend and (ii) the rain gauge data to form local residuals that are spatially interpolated and added to the trend. Since the station locations of the two networks do not coincide, the concept of pseudo cross-variogram is employed to compute the linear model of coregionalization

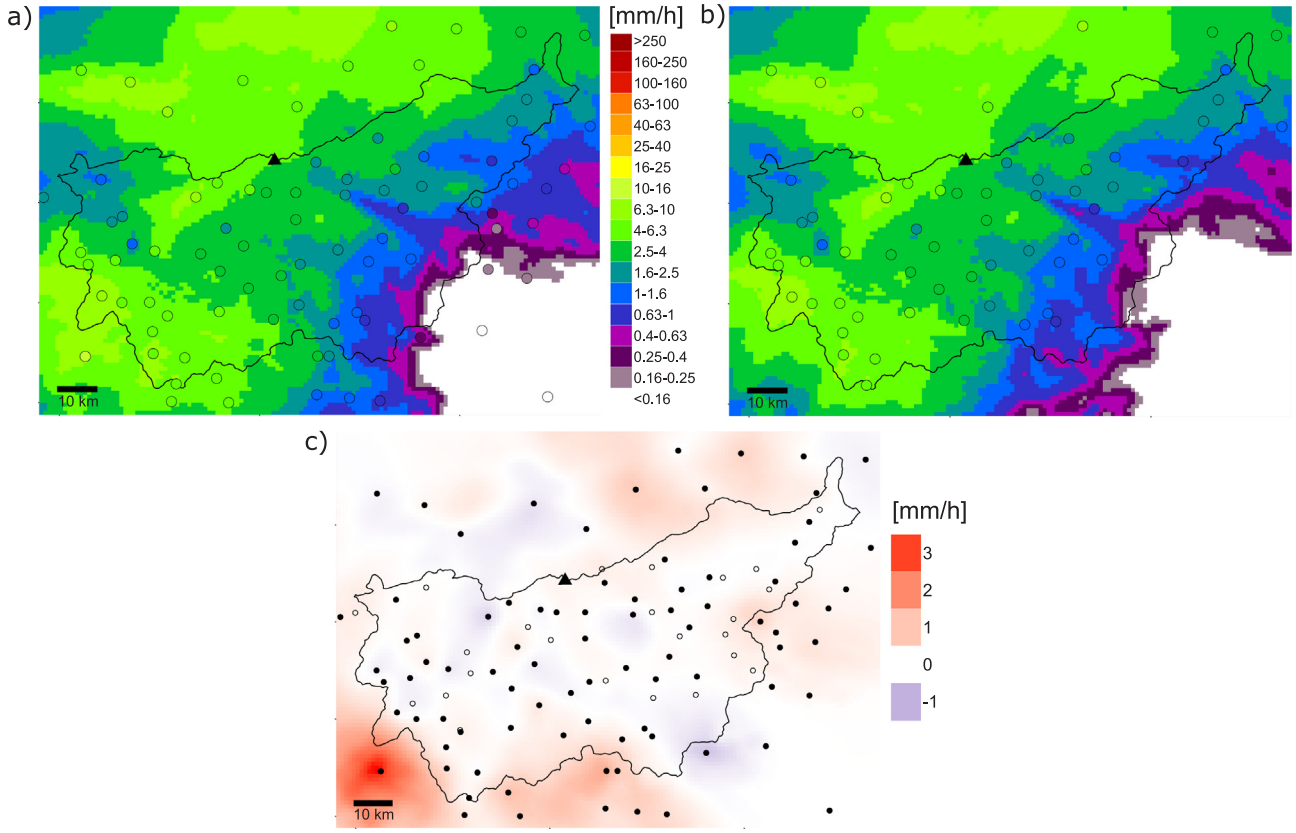


**Fig. 13.** Hourly precipitation interpolated using RCK(SMN,MG) (a) considering all station networks around the basin (see Table 1) together with the SMN stations as a single (primary) variable (time step: 01-05-2015 2200 UTC + 1); (b) as (a) but without surroundings station networks; (c) difference between (a) and (b). On (a) and (b), the circles represent the primary stations. On (c), the filled circles represent primary stations, the empty circles the secondary stations. The triangle represents the location of the radar of Pointe de la Plaine Morte.

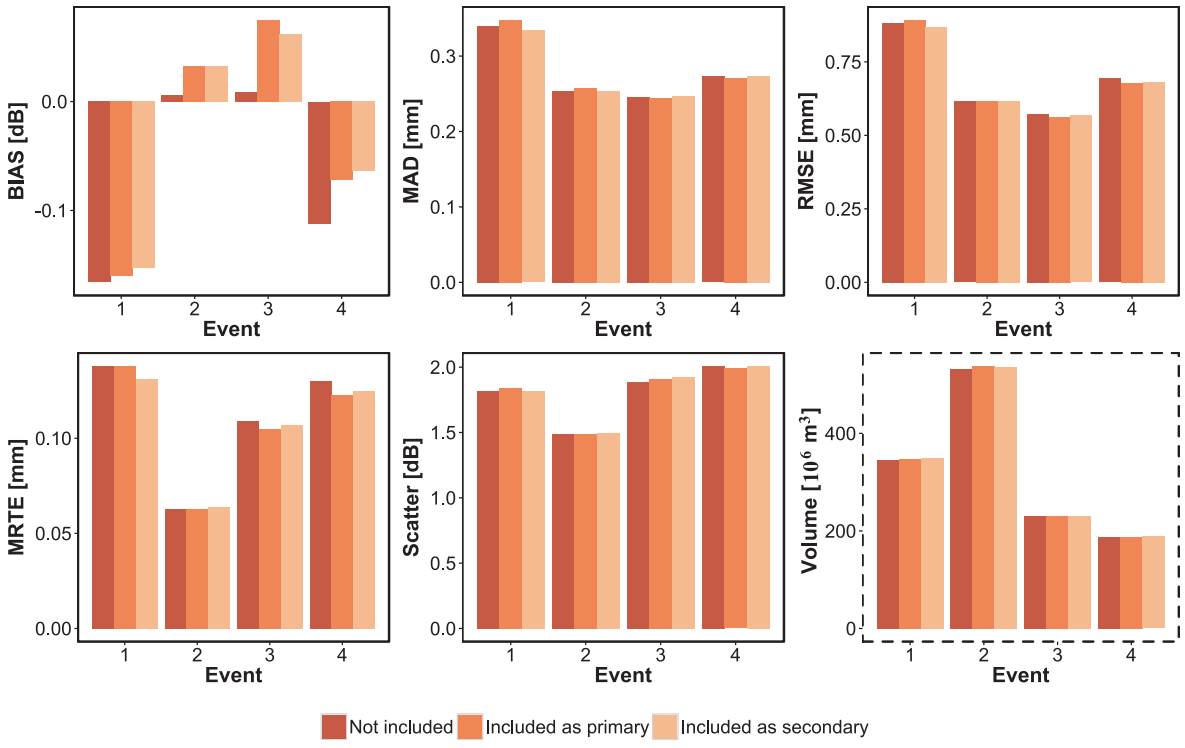


**Fig. 14.** Performance indicators comparison for RCK(SMN,MG) including or not the neighbouring networks, and using them as primary, respectively secondary network.

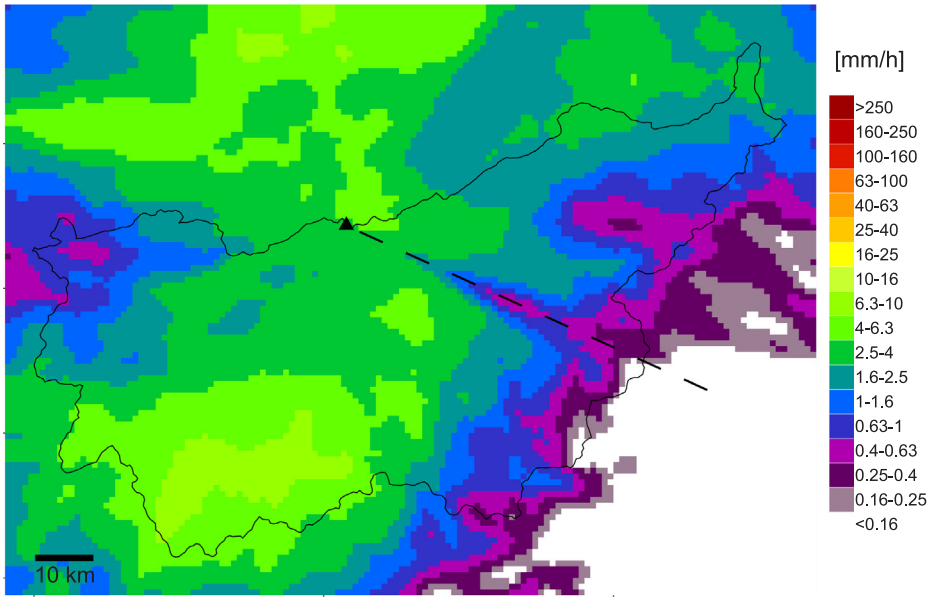


**Fig. 15.** Example of a raw radar data with the blind zone in south-east direction of the radar of Pointe de la Plaine Morte (time step: 01-05-2015 2200 UTC + 1). The black triangle represents the weather radar. The dashed-line indicates the blind zone direction.

used for the co-kriging interpolation.

The completed detailed tests demonstrated that regression co-kriging using the SMN data as primary variable and MG data as secondary variable to interpolate the local precipitation residuals provides the best performance for the study area. The method even proved to clearly outperform the Inverse distance weighting method for historical data availability scenarios, before the radar network was completed and with lower rain gauge station density. This result is important for hydrological applications where data over many years are required. The gain introduced by the co-kriging approach is demonstrated by showing a bias issue when considering both networks jointly linked to a difference in the networks quality. Regardless of the spatial scale, data combination must therefore consider with care the quality of the sensors providing the data when elaborating a combination methodology. The results of the analysis also showed that even with up-to-date modern weather radar equipments, radar-gauge combination in a complex topography such as the Swiss Alps requires a high-level treatment of the data. This is particularly true for reducing the artefacts due to beam shielding by the topography.

An interesting side-result of this study is the fact that if a single rain gauge network (SMN stations) is combined with radar data, a kriging-based residual interpolation does not clearly outperform a simple inverse distance weighting of the residuals. This is probably explained, at least partly, by the relatively low number of rain gauges that report precipitation for some time steps over the considered domain, which is often near the limit or even below the minimum required number to obtain robust variograms (which is particularly limiting for RCK where two variables need to meet this criterion).

Overall, the presented results underline the importance of analyzing in detail the evolving data situation to propose robust precipitation interpolation methods. This not only holds for regions where the rain gauge and radar network is evolving; any existing network might indeed suffer from device failures and ensuing missing data.

In general, the detailed analysis of different rain gauge networks provided here (including networks of neighbouring regions, networks of different quality), illustrates that integration of several networks for operational interpolation purposes is not straightforward. Since the available meteorological data (quantity and quality) is permanently increasing, there is ample room for further studies on improving quantitative precipitation estimates for complex Alpine environments. Based on our analysis, the most promising research direction is certainly the pre-processing of the radar data in particular to account for known beam shielding effects and to take advantage of recent progress in the field of hydrometeor type classification for radar data.

## Acknowledgments

The research project from which this article results is realized at the Ecole Polytechnique Fédérale de Lausanne (EPFL) in Switzerland, and is co-funded by the Centre de recherche sur l'environnement alpin (CREALP), located in Sion (Switzerland), and the Swiss Federal Office of Energy (SFOE). The authors express their gratitude to all involved stakeholders: the Canton of Valais, the Swiss Federal Office for Meteorology and Climatology (MeteoSwiss), the Universitat Politècnica de València and the engineering office HydroCosmos SA. The meteorological data used within the project come from the SwissMetNet network from MeteoSwiss, as well as the networks of the private company MeteoGroup Switzerland AG, the Canton of Bern, Météo-France, Electricité de France, the Regione Autonoma Valle d'Aosta and the ARPA Piemonte. The radar data have been provided by MeteoSwiss. We thank all the different data providers. Acknowledgments also go to the CREALP colleagues who collaborate on the MINERVE system and contributed to the set-up of the hydrometeorological database used for the study. Prof. Alexis Berne from the Environmental Remote Sensing Laboratory at EPFL and Dr. Ioannis Sideris from MeteoSwiss are also acknowledged for their inputs and feedback on the manuscript.

## Appendix A. Supplementary data

Supplementary data associated with this article can be found, in the online version, at http://dx.doi.org/10.1016/j.jhydrol.2018.05.027.

## References

Agroscope, 2017. Agrometeo - Prévision et gestion des risques pour l'agriculture,www.agrometeo.ch, [Online]. Accessed: 13-Sep-2017.

Ahmed, S., De Marsily, G., 1987. Comparison of geostatistical methods for estimating transmissivity using data on transmissivity and specific capacity. Water Resour. Res. 23 (9), 1717–1737. http://dx.doi.org/10.1029/WR023i009p01717.

Alsamamra, H., Ruiz-Arias, J.A., Pozo-Vázquez, D., Tovar-Pescador, J., 2009. A comparative study of ordinary and residual kriging techniques for mapping global solar radiation over southern Spain. Agric. For. Meteorol. 149 (8), 1343–1357. http://dx.doi.org/10.1016/j.agrformet.2009.03.005.

Attinger, S., Fallot, J., 2003. Fréquence des intempéries et des précipitations abondantes

en Valais (Alpes Suisses Occidentales) durant le 20ème siècle. Association Int. de Climatol 15, 253–259.
Bárdossy, A., Pegram, G., 2013. Interpolation of precipitation under topographic influence at different time scales. Water Resour. Res. 49 (8), 4545–4565. http://dx.doi.org/10.1002/wrcr.20307.
Berndt, C., Rabiei, E., Haberlandt, U., 2014. Geostatistical merging of rain gauge and radar data for high temporal resolutions and various station density scenarios. J. Hydrol. 508, 88–101. http://dx.doi.org/10.1016/j.jhydrol.2013.10.028.
Berne, A., Krajewski, W.F., 2013. Radar for hydrology: unfulfilled promise or unrecognized potential? Adv. Water Resour. 51, 357–366. http://dx.doi.org/10.1016/j.advwatres.2012.05.005.
Bérod, D., 2013. Estimation et prévision des crues en Valais, Tech. Rep., Swiss Hydrological Commission (CHy), Bern.
Cantet, P., 2017. Mapping the mean monthly precipitation of a small island using kriging with external drifts. Theoret. Appl. Climatol. 127 (1–2), 31–44. http://dx.doi.org/10.1007/s00704-015-1610-z.
Cecinati, F., Moreno Ródenas, M., Rico-Ramirez, M.A., 2017a. Integration of rain gauge errors in radar-rain gauge merging techniques, in: 10th World Congress on Water Resources and Environment, Athens, 279–285.
Cecinati, F., Wani, O., Rico-Ramirez, M.A., 2017b. Comparing approaches to deal with non-gaussianity of rainfall data in kriging-based radar-gauge rainfall merging. Water Resour. Res. (00431397) 53 (11), 8999–9018. http://dx.doi.org/10.1002/2016WR020330.
Ciach, G.J., Krajewski, W.F., 1999. On the estimation of radar rainfall error variance. Adv. Water Resour. 22 (6), 585–595. http://dx.doi.org/10.1016/S0309-1708(98)00043-8.
Creutin, J.D., Delrieu, G., Lebel, T., 1988. Rain measurement by raingage-radar combination: a geostatistical approach. J. Atmos. Oceanic Technol. 5 (1), 102–115. http://dx.doi.org/10.1175/1520-0426(1988) 0050102:RMBRRC2.0.CO;2.
Delhomme, J., 1978. Kriging in the hydrosciences. Adv. Water Resour. 1 (5), 251–266. http://dx.doi.org/10.1016/0309-1708(78)90039-8.
Di Piazza, A., Conti, F.L., Noto, L., Viola, F., La Loggia, G., 2011. Comparative analysis of different techniques for spatial interpolation of rainfall data to create a serially complete monthly time series of precipitation for Sicily, Italy. Int. J. Appl. Earth Observation Geoinform. 13 (3), 396–408. http://dx.doi.org/10.1016/j.jag.2011.01.005.
Egli, L., Jonas, T., Meister, R., 2009. Comparison of different automatic methods for estimating snow water equivalent. Cold Regions Sci. Technol. 57 (2–3), 107–115. http://dx.doi.org/10.1016/j.coldregions.2009.02.008. ISSN 0165232X.
Ehret, U., 2003. Rainfall and flood nowcasting in small catchments using weather radar, no. Heft 121 in Mitteilungen des Instituts für Wasserbau, Universität Stuttgart, Stuttgart, ISBN 978-3-933761-24-8.
Erdin, R., Frei, C., Künsch, H.R., 2012. Data transformation and uncertainty in geostatistical combination of Radar and Rain Gauges. J. Hydrometeorol. 13 (4), 1332–1346. http://dx.doi.org/10.1175/JHM-D-11-096.1.
Fischer, M., Huss, M., Hoelzle, M., 2015. Surface elevation and mass changes of all Swiss glaciers 1980–2010. Cryosphere 9 (2), 525–540. http://dx.doi.org/10.5194/tc-9-525-2015.
Foehn, A., García Hernández, J., Schaefli, B., De Cesare, G., Schleiss, A.J., 2016. Spatialization of precipitation data for flood forecasting applied to the Upper Rhone River basin. In: International Conference Hydro 2016, Montreux.
FOEN, 2017a. Hydrological data and forecasts, Federal Office for the Environment FOEN, http://hydrodaten.admin.ch/en/, [Online]. Accessed: 13-Oct-2017.
FOEN, 2017b. 10 minutes average discharge data.
Gabella, M., Speirs, P., Hamann, U., Germann, U., Berne, A., 2017. Measurement of precipitation in the alps using dual-polarization C-band ground-based radars, the GPM spaceborne Ku-Band Radar, and Rain Gauges. Remote Sensing 9 (11). http://dx.doi.org/10.3390/rs9111147. ISSN 2072-4292.
García Hernández, J. 2011a. Flood management in a complex river basin with a real-time decision support system based on hydrological forecasts, PhD Thesis N° 5093, Ecole Polytechnique Fédérale de Lausanne, Lausanne.
García Hernández, J., 2011b. Flood management in a complex river basin with a real-time decision support system based on hydrological forecasts, Communication 48 du Laboratoire de Constructions Hydrauliques, Ed. A. Schleiss, EPFL, Lausanne.
García Hernández, J., Boillat, J.-L., Jordan, F., Hingray, B., 2009. La prévision hydrométéorologique sur le bassin versant du Rhône en amont du Léman. La Houille Blanche 5, 61–70. http://dx.doi.org/10.1051/lhb/2009057.
García Hernández, J., Claude, A., Paredes Arquiola, J., Roquier, B., Boillat, J.-L., 2014. Integrated flood forecasting and management system in a complex catchment area in the Alps – implementation of the MINERVE project in the Canton of Valais. In: Schleiss, A., Speerli, J., Pfammatter, R. (Eds.), Swiss Competences in River Engineering and Restoration. CRC Press, pp. 87–97 ISBN 978-1-138-02676-6 et 978-1-4987-0443-4, 2014.
García Hernández, J., Jordan, F., Dubois, J., Boillat, J.-L. 2007. Routing System II - Modélisation d'écoulements dans des systèmes hydrauliques, Communication 32 du Laboratoire de Constructions Hydrauliques, Ed. A. Schleiss, EPFL, Lausanne.
Germann, U., Galli, G., Boscacci, M., Bolliger, M., 2006. Radar precipitation measurement in a mountainous region. Q. J. R. Meteorolog. Soc. 132 (618), 1669–1692. http://dx.doi.org/10.1256/qj.05.190.
Germann, U., Berenguer, M., Sempere-Torres, D., Zappa, M., 2009. REAL-Ensemble radar precipitation estimation for hydrology in a mountainous region. Q. J. R. Meteorolog. Soc. 135 (639), 445–456. http://dx.doi.org/10.1002/qj.375.
Germann, U., Boscacci, M., Gabella, M., Sartori, M., 2015. Peak performance – Radar design for prediction in the Swiss Alps – The latest fourth-generation MeteoSwiss weather radar network is called Rad4Alp. Meteorolog. Technol. Int. 42–45.
Goovaerts, P. 1997. Geostatistics for natural resources evaluation, Applied geostatistics series, Oxford University Press, New York, ISBN 978-0-19-511538-3.
Goovaerts, P., 2000. Geostatistical approaches for incorporating elevation into the spatial interpolation of rainfall. J. Hydrol. 228 (1–2), 113–129. http://dx.doi.org/10.1016/S0022-1694(00)00144-X.
Goudenhoofdt, E., Delobbe, L., 2009. Evaluation of radar-gauge merging methods for quantitative precipitation estimates. Hydrol. Earth Syst. Sci. 13 (2), 195–203. http://dx.doi.org/10.5194/hess-13-195-2009.
Grazioli, J., Tuia, D., Berne, A., 2015. Hydrometeor classification from polarimetric radar measurements: a clustering approach. Atmos. Measure. Tech. 8 (1), 149–170. http://dx.doi.org/10.5194/amt-8-149-2015.
Haberlandt, U., 2007. Geostatistical interpolation of hourly precipitation from rain gauges and radar for a large-scale extreme rainfall event. J. Hydrol. 332 (1–2), 144–157. http://dx.doi.org/10.1016/j.jhydrol.2006.06.028.
Hengl, T., Heuvelink, G.B., Rossiter, D.G., 2007. About regression-kriging: From equations to case studies. Comput. Geosci. 33 (10), 1301–1315. http://dx.doi.org/10.1016/j.cageo.2007.05.001.
Hingray, B., Schaefli, B., Mezghani, A., Hamdi, Y., 2010. Signature-based model calibration for hydrological prediction in mesoscale Alpine catchments. Hydrol. Sci. J. 55 (6), 1002–1016. http://dx.doi.org/10.1080/02626667.2010.505572.
Jewell, S.A., Gaussiat, N., 2015. An assessment of kriging-based rain-gauge-radar merging techniques: Gauge-Radar Merging Schemes for Flood Forecasting. Q. J. R. Meteorolog. Soc. 141 (691), 2300–2313. http://dx.doi.org/10.1002/qj.2522. ISSN 00359009.
Jordan, F. 2007a. Modèle de prévision et de gestion des crues: optimisation des opérations des aménagements hydroélectriques à accumulation pour la réduction des débits de crue, Communication 29 du Laboratoire de Constructions Hydrauliques, Ed. A. Schleiss, EPFL, Lausanne.
Jordan, F. 2007b. Modèle de prévision et de gestion des crues: optimisation des opérations des aménagements hydroélectriques à accumulation pour la réduction des débits de crue, PhD Thesis N° 3711, Ecole Polytechnique Fédérale de Lausanne, Lausanne.
Jordan, F., Boillat, J.-L., Schleiss, A., 2010. Prévision et gestion des crues du Rhône supérieur par l'exploitation optimale des retenues alpines. La Houille Blanche 5, 91–102. http://dx.doi.org/10.1051/lhb/2010060.
Jordan, F.M., Boillat, J.-L., Schleiss, A.J., 2012. Optimization of the flood protection effect of a hydropower multi-reservoir system. Int. J. River Basin Manage. 10 (1), 65–72. http://dx.doi.org/10.1080/15715124.2011.650868.
Lanza, L.G., Vuerich, E., 2009. The WMO field intercomparison of rain intensity gauges. Atmos. Res. 94 (4), 534–543. http://dx.doi.org/10.1016/j.atmosres.2009.06.012.
Ly, S., Charles, C., Degré, A., 2011. Geostatistical interpolation of daily rainfall at catchment scale: the use of several variogram models in the Ourthe and Ambleve catchments, Belgium. Hydrology Earth System Sci. 15 (7), 2259–2274. http://dx.doi.org/10.5194/hess-15-2259-2011.
Ly, S., Charles, C., Degre, A., 2013. Different methods for spatial interpolation of rainfall data for operational hydrology and hydrological modeling at watershed scale. A review. Biotechnol. Agron. Soc. Environ. 17 (2), 392–406.
Marty, C., 2008. Regime shift of snow days in Switzerland. Geophys. Res. Lett. 35 (12), 1–5. http://dx.doi.org/10.1029/2008GL033998.
Matheron, G. 1971. The theory of regionalized variables and its applications, Tech. Rep., Paris: École Nationale Supérieure des Mines de Paris.
Messer, H., Zinevich, A., Alpert, P., 2006. Environmental monitoring by wireless communication networks. Science 312 (5774), 713. http://dx.doi.org/10.1126/science.1120034. ISSN 0036-8075, 1095–9203.
MeteoSwiss, 2012. Nouveau radar météorologique pour la Suisse alémanique, Press release, http://www.meteosuisse.admin.ch/home/actualite/infos.subpage.html/fr/data/news/2012/4/nouveau-radar-meteorologique-pour-la-suisse-alemanique.html?query=radar&topic=0&dateRange=all&dateFrom=&dateTo=, 2012.
MeteoSwiss, 2014a. Räumliche Daten CombiPrecip, Federal Office of Meteorology and Climatology, http://www.meteoswiss.admin.ch/home/search.subpage.html/en/data/products/2014/raeumliche-daten-combiprecip.html, 1-Dec-2014. [Online]. Accessed: 10-Oct-2017.
MeteoSwiss, 2014b. Climate diagrams and normal values per station, Federal Office of Meteorology and Climatology, http://www.meteoswiss.admin.ch/home/climate/past/climate-normals/climate-diagrams-and-normal-values-per-station.html, 1-Dec-2014. [Online]. Accessed: 11-Oct-2017.
MeteoSwiss, 2014c. De nouveaux radars météorologiques pour la Suisse, Press release, http://www.meteosuisse.admin.ch/home/actualite/infos.subpage.html/fr/data/news/2014/5/de-nouveaux-radars-meteorologiques-pour-la-suisse.html?query=de+nouveaux+radars&topic=0&dateRange=all&dateFrom=&dateTo=.
MeteoSwiss, 2015. Measurement instruments, Federal Office of Meteorology and Climatology, http://www.meteoswiss.admin.ch/home/measurement-and-forecasting-systems/land-based-stations/automatisches-messnetz/measurement-instruments.html, 23-Nov-2015. [Online]. Accessed: 2-Oct-2017.
MeteoSwiss, 2016a. Automatic monitoring network, Federal Office of Meteorology and Climatology, http://www.meteoswiss.admin.ch/home/measurement-and-forecasting-systems/land-based-stations/automatisches-messnetz.html, 17-Aug-2016. [Online]. Accessed: 19-Sep-2017.
MeteoSwiss, 2016b. Project Rad4Alp – A modern radar network for Switzerland, http://www.meteoswiss.admin.ch/content/dam/meteoswiss/en/Mess-Prognosesysteme/doc/Rad4Alpen.pdf, Feb-2016. [Online]. Accessed: 13-Oct-2017.
MeteoSwiss, 2016c. Le réseau de radars météorologiques de la Suisse est achevé, Press release, http://www.meteosuisse.admin.ch/home/actualite/infos.subpage.html/fr/data/news/2016/2/le-reseau-de-radars-meteorologiques-de-la-suisse-est-acheve.html.
MeteoSwiss, 2016d. Extreme value analyses (version 2016) - Standard period 1966–2015, Federal Office of Meteorology and Climatology, http://www.meteoswiss.admin.ch/home/climate/past/climate-extremes/extreme-value-analyses/standard-period.

html?, 12-May-2016. [Online]. Accessed: 17-Aug-2017.
MeteoSwiss, 2017. COSMO-7 – the model for western and central Europe, Federal Office of Meteorology and Climatology, http://www.meteoswiss.admin.ch/home/measurement-and-forecasting-systems/warning-and-forecasting-systems/cosmo-forecasting-system/cosmo-7-the-model-for-western-and-central-europe.html, 16-Mar-2017. [Online]. Accessed: 21-Sep-2017.
Musa, M., Grüter, E., Abbt, M., Häberli, C., Häller, E., Küng, U., Konzelmann, T., Dössegger, R., 2003. Quality control tools for meteorological data in the MeteoSwiss Datawarehouse system. Internal report. MeteoSwiss, Zürich.
Myers, D.E., 1982. Matrix formulation of co-kriging. J. Int. Assoc. Math. Geol. 14 (3), 249–257. http://dx.doi.org/10.1007/BF01032887.
Nešpor, V., Sevruk, B., 1999. Estimation of wind-induced error of rainfall gauge measurements using a numerical simulation. J. Atmos. Oceanic Technol. 16 (4), 450–464. http://dx.doi.org/10.1175/1520-0426(1999)016<0450:EOWIEO>2.0.CO;2.
Odeh, I., McBratney, A., Chittleborough, D., 1995. Further results on prediction of soil properties from terrain attributes: heterotopic cokriging and regression-kriging. Geoderma 67 (3–4), 215–226. http://dx.doi.org/10.1016/0016-7061(95)00007-B.
Pebesma, E. 2014. Gstat User's Manual,http://www.gstat.org/gstat.pdf.
Pebesma, E., Graeler, B. 2017. Package 'gstat', version 1.1-3.
Phillips, D.L., Dolph, J., Marks, D., 1992. A comparison of geostatistical procedures for spatial analysis of precipitation in mountainous terrain. Agric. For. Meteorol. 58 (1–2), 119–141. http://dx.doi.org/10.1016/0168-1923(92)90114-J.
R Core Team, 2016. R: A Language and Environment for Statistical Computing, R Foundation for Statistical Computing, Vienna, Austria, ISBN 3-900051-07-0,https://www.R-project.org/.
Savina, M., Schäppi, B., Molnar, P., Burlando, P., Sevruk, B., 2012. Comparison of a tipping-bucket and electronic weighing precipitation gage for snowfall. Atmos. Res. 103, 45–51. http://dx.doi.org/10.1016/j.atmosres.2011.06.010.
Schiemann, R., Erdin, R., Willi, M., Frei, C., Berenguer, M., Sempere-Torres, D., 2011. Geostatistical radar-raingauge combination with nonparametric correlograms: methodological considerations and application in Switzerland. Hydrol. Earth Syst. Sci. 15 (5), 1515–1536. http://dx.doi.org/10.5194/hess-15-1515-2011.
Schuurmans, J.M., Bierkens, M.F.P., Pebesma, E.J., Uijlenhoet, R., 2007. Automatic prediction of high-resolution daily rainfall fields for multiple extents: the potential of operational radar. J. Hydrometeorol. 8 (6), 1204–1224. http://dx.doi.org/10.1175/2007JHM792.1.
Shepard, D., 1968. A Two-dimensional Interpolation Function for Irregularly-spaced Data ACM Presshttp://dx.doi.org/10.1145/800186.810616. pp. 517–524.
Sideris, I.V., Gabella, M., Erdin, R., Germann, U., 2014a. Real-time radar-rain-gauge merging using spatio-temporal co-kriging with external drift in the alpine terrain of Switzerland: Real-time radar-rain-gauge merging. Q. J. R. Meteorolog. Soc. 140 (680), 1097–1111. http://dx.doi.org/10.1002/qj.2188.
Sideris, I.V., Gabella, M., Sassi, M., Germann, U. 2014b. The CombiPrecip experience: development and operation of a real-time radar-raingauge combination scheme in Switzerland, in: 2014 International Symposium Weather Radar and Hydrology, Washington DC.
Sikorska, A., Seibert, J., 2018. Value of different precipitation data for flood prediction in an alpine catchment: a Bayesian approach. J. Hydrol. 556, 961–971. http://dx.doi.org/10.1016/j.jhydrol.2016.06.031.
SLF, 2017. Intercantonal Measurement and Information System (IMIS), WSL Institute for Snow and Avalanche Research SLF, http://www.slf.ch/ueber/organisation/warnungpraevention/warninformationssysteme/messnetzedaten/imis/indexEN, [Online]. Accessed: 11-Oct-2017.
Smiatek, G., Keis, F., Chwala, C., Fersch, B., Kunstmann, H., 2017. Potential of commercial microwave link network derived rainfall for river runoff simulations. Environ. Res. Lett. 12 (3). http://dx.doi.org/10.1088/1748-9326/aa5f46. ISSN 1748-9326.
Speirs, P., Gabella, M., Berne, A., 2017. A comparison between the GPM dual-frequency precipitation radar and ground-based radar precipitation rate estimates in the Swiss Alps and Plateau. J. Hydrometeorol. 18 (5), 1247–1269. http://dx.doi.org/10.1175/JHM-D-16-0085.1. ISSN 1525-755X, 1525-7541.
Swisstopo, 2005. DHM25 – The digital height model of Switzerland.
Swisstopo, 2012. Swiss Map Raster 1000 – National map of switzerland 1:1million.
Swisstopo, 2013. swissTLM3D – large-scale topographical landscape model of Switzerland.
Swisstopo, 2017a. Vector200 – The small-scale landscape model of Switzerland.
Swisstopo, 2017b. swissBOUNDARIES3D - Administrative units of Switzerland.
Thiessen, A.H., 1911. Precipitation averages for large areas. Mon. Weather Rev. 39 (7), 1082–1089. http://dx.doi.org/10.1175/1520-0493(1911)391082b:PAFLA2.0.CO;2.
Tobin, C., 2012. Improving alpine flood prediction through hydrological process characterization and uncertainty analysis, PhD Thesis N° 5416, Ecole Polytechnique Fédérale de Lausanne, Lausanne.
Tobin, C., Nicotina, L., Parlange, M.B., Berne, A., Rinaldo, A., 2011. Improved interpolation of meteorological forcings for hydrologic applications in a Swiss Alpine region. J. Hydrol. 401 (1–2), 77–89. http://dx.doi.org/10.1016/j.jhydrol.2011.02.010.
Upton, G., Rahimi, A., 2003. On-line detection of errors in tipping-bucket raingauges. J. Hydrol. 278 (1–4), 197–212. http://dx.doi.org/10.1016/S0022-1694(03)00142-2. ISSN 00221694.
Verdin, A., Rajagopalan, B., Kleiber, W., Funk, C., 2015. A Bayesian kriging approach for blending satellite and ground precipitation observations. Water Resour. Res. 51 (2), 908–921. http://dx.doi.org/10.1002/2014WR015963.
Villarini, G., Krajewski, W.F., 2010. Review of the different sources of uncertainty in single polarization radar-based estimates of rainfall. Surveys Geophys. 31 (1), 107–129. http://dx.doi.org/10.1007/s10712-009-9079-x. ISSN 0169–3298, 1573–1956.
Villarini, G., Mandapaka, P.V., Krajewski, W.F., Moore, R.J., 2008. Rainfall and sampling uncertainties: a rain gauge perspective. J. Geophys. Res. 113, 1–12. http://dx.doi.org/10.1029/2007JD009214.
Vogl, S., Laux, P., Qiu, W., Mao, G., Kunstmann, H., 2012. Copula-based assimilation of radar and gauge information to derive bias-corrected precipitation fields. Hydrol. Earth Syst. Sci. 16 (7), 2311–2328. http://dx.doi.org/10.5194/hess-16-2311-2012.
Vuerich, E., Monesi, C., Lanza, L., Stagi, L., Lanzinger, E., 2009. WMO Field intercomparison of rainfall intensity gauges, Instruments and observing methods Report no. 99, World Meteorological Organization, Vigna di Valle, Italy.
Wagner, P.D., Fiener, P., Wilken, F., Kumar, S., Schneider, K., 2012. Comparison and evaluation of spatial interpolation schemes for daily rainfall in data scarce regions. J. Hydrol. 464–465, 388–400. http://dx.doi.org/10.1016/j.jhydrol.2012.07.026.
Webster, R., Oliver, M.A., 2007. 2nd edn. Geostatistics for environmental scientists, Statistics in practice Wiley, Chichester978-0-470-02858-2.